Corticospinal Interface to Restore Voluntary Control of Joint Torque in a Paralyzed Forearm Following Spinal Cord Injury in Non-Human Primates

Kei Obara[1,2], Miki Kaneshige[1], Michiaki Suzuki[1], Osamu Yokoyama[1], Toshiki Tazoe[1], Yukio Nishimura[1,2*]

[1]Neural Prosthetics Project, Tokyo Metropolitan Institute of Medical Science, Setagaya, Tokyo 156-8506, Japan.
[2]Division of Neural Engineering, Graduate School of Medical and Dental Sciences, Niigata University, Niigata, Niigata 951-8510, Japan.

* Correspondence
Yukio Nishimura
E-mail: nishimura-yk@igakuken.or.jp

Running title: Corticospinal interface in spinal cord injury

23 **Abstract**

24   The corticospinal tract plays a major role in the control of voluntary limb movements,
25   and its damage impedes voluntary limb control. We investigated the feasibility of closed-
26   loop brain-controlled subdural spinal stimulation through a corticospinal interface for the
27   modulation of wrist torque in the paralyzed forearm of monkeys with spinal cord injury
28   at C4/C5. Subdural spinal stimulation of the preserved cervical enlargement activated
29   multiple muscles on the paralyzed forearm and wrist torque in the range from flexion to
30   ulnar-flexion. The magnitude of the evoked torque could be modulated by changing
31   current intensity. We then employed the corticospinal interface designed to detect the
32   firing rate of an arbitrarily selected "linked neuron" in the forearm territory of the primary
33   motor cortex (M1) and convert it in real time to activity-contingent electrical stimulation
34   of a spinal site caudal to the lesion. Linked neurons showed task-related activity that
35   modulated the magnitude of the evoked torque and the activation of multiple muscles
36   depending on the required torque. Unlinked neurons, which were independent of spinal
37   stimulation and located in the vicinity of the linked neurons, exhibited task-related or -
38   unrelated activity. Thus, monkeys were able to modulate the wrist torque of the paralyzed
39   forearm by modulating the firing rate of M1 neurons including unlinked and linked
40   neurons via the corticospinal interface. These results suggest that the corticospinal
41   interface can replace the function of the corticospinal tract after spinal cord injury.

42

43 **1 Introduction**

44 The disruption of descending pathways including the corticospinal tract results in the

45 loss of connection between the brain and spinal networks and the consequent loss of

46 voluntary motor function. However, the neural circuits located above and below the

47 lesion retain their functions. Electrical stimulation of the spinal cord is a promising

48 method to restore voluntary motor function after the impairment of descending

49 pathways through spinal cord injury (SCI) or stroke. Tonic electrical stimulation of the

50 spinal cord below the lesion has been shown to improve motor function in humans

51 (Minassian et al., 2004; Harkema et al., 2011; Angeli et al., 2014; Lu et al., 2016;

52 Inanici et al., 2018) and animals (Musienko et al., 2009; Kasten et al., 2013; Mondello

53 et al., 2014; Alam et al., 2015) with SCI in which residual descending motor pathways

54 are assumed. Tonic spinal stimulation can raise the excitability of the spared spinal

55 circuits and compensate for the weakened descending commands, which are insufficient

56 for voluntary motor output (Angeli et al., 2014; Rejc et al., 2015; Lu et al., 2016; Gad et

57 al., 2017). Therefore, even uncontrolled open-loop tonic spinal stimulation is useful for

58 the restoration of voluntary motor function in patients with residual descending

59 pathways. In contrast, it is impossible for patients who have completely lost their

60 descending pathways to voluntarily control their paralyzed limb movements by tonic

61 spinal stimulation, even though substantial muscle contractions are produced.

62 Bypassing the damaged descending pathway using brain-controlled functional electrical

63 stimulation is a promising approach to restore the voluntary control of paralyzed limb

64 movements after the complete loss of descending pathways (Moritz et al., 2008;

65 Pohlmeyer et al., 2009; Ethier et al., 2012; Nishimura et al., 2013; Zimmermann and

66 Jackson, 2014; Bouton et al., 2016; Ajiboye et al., 2017; Kato et al., 2019; Barra et al.,

67 2022). Until recently, the self-execution of paralyzed upper limb movements such as

68 wrist flexion, grasping, and arm retraction has been achieved by brain-controlled

69 functional electrical stimulation of the spinal cord in paralyzed monkeys (Nishimura et

70 al., 2013; Zimmermann and Jackson, 2014; Barra et al., 2022). However, the graded

71 control of force by brain-controlled spinal stimulation has yet to be achieved. Therefore,

72 it is worthwhile assessing the feasibility of brain-controlled spinal stimulation for the

73 modulation of motor output.

74 Here, we investigated the feasibility of a corticospinal interface through closed-loop

75 brain-controlled subdural spinal stimulation for the modulation of motor output in the

76 paralyzed hand of monkeys with SCI. We found that paralyzed monkeys could modulate

77   motor output such as wrist torque and the activation of multiple forearm muscles by

78   modulating the firing rate of an ensemble of neurons in the primary motor cortex (M1)

79   via the corticospinal interface, indicating that a corticospinal interface can compensate

80   for the function of a lesioned corticospinal tract.

81

82 **2 Materials and Methods**

83 **2.1 Subjects**

84 The experiments were performed using two female macaque monkeys (*Macaca fuscata*:

85 Monkey E, 5.6 kg and Monkey L, 5.0 kg). All experimental procedures were performed

86 in accordance with the guidelines for the Care and Use of Nonhuman Primates in

87 Neuroscience Research, The Japan Neuroscience Society, and were approved by the

88 Institutional Animal Care and Use Committee of the Tokyo Metropolitan Institute of

89 Medical Science (Approval Nos.: 18035, 19050, and 20-053). The animals were fed

90 regularly with pellets and had free access to water. They were monitored closely and

91 animal welfare was assessed daily or, if necessary, several times a day.

92

93 **2.2 Surgery**

94 All surgical procedures were performed in sterile conditions under general anesthesia

95 induced by ketamine (10 mg/kg, i.m.) plus xylazine (1 mg/kg, i.m.) and maintained with

96 1–1.5% isoflurane. Atropine (0.12 mg/kg, i.m.), ketoprofen (2 mg/kg, i.m.), maropitant

97 (1 mg/kg, s.c.), and ampicillin (40 mg/kg, i.m.) were administered preoperatively. The

98 depth of anesthesia was confirmed by the pain response. During anesthesia, the animal's

99 vital signs (respiratory rate, inspiratory CO_2 concentration, saturation of percutaneous

100 O_2, heart rate, and body temperature) were monitored carefully. There was no evidence

101 of tachycardia or tachypnea during the surgical procedures nor a major deviation in the

102 heart or respiratory rate in response to noxious stimuli. The absence of reflexive

103 movements to noxious stimuli and corneal reflex was also used to verify the level of

104 anesthesia. Postoperative management consisted of observing the animals until they

105 were completely recovered from the anesthesia, and the administration of ampicillin (40

106 mg/kg, i.m.), ketoprofen (2.0 mg/kg, i.m.), and dexamethasone (0.825 mg, i.m.).

107 **2.2.1 Cortical array implantation**

108 To record cell activity in M1, we chronically implanted a 96-channel iridium-oxide

109 Utah array (Blackrock Microsystems, Salt Lake City, UT, USA) with an electrode

110 length of 1.5 mm. The array was implanted in the wrist area of the left M1, which was

111 identified by anatomical features and movements evoked by trains of low-intensity

112   electrical stimulation to the cortical surface. The reference electrodes were placed in the
113   subdural space. The ground electrode and connector of the arrays and head-post were
114   anchored to the skull with titanium screws and acrylic cement.

115   **2.2.2 Spinal cord lesioning and electrode implantation on the cervical cord**

116   Under anesthesia, the border between the C4 and C5 segments was exposed by
117   laminectomy of the C3 and C4 vertebrae, and a transverse opening was made in the
118   dura. A spinal cord lesion was made by transecting the dorsolateral funiculus and dorsal
119   column at the border between C4 and C5 on the right side (Fig. 1A-C) under a surgical
120   microscope using fine forceps.

121   After spinal cord lesioning, incisions were made in the dura mater on the C4 and C7
122   vertebrae. A 6-channel platinum subdural electrode array, with an electrode diameter of
123   1 mm and inter-electrode distance of 3 mm (Unique Medical Corporation, Tokyo,
124   Japan), was implanted on the right side of the cervical enlargement (C6–T1). The array
125   was slid into the subdural space from the incision site at the C7 vertebra, and placed
126   over the dorsal-lateral aspect of the C6–T1 segments, where the dorsal rootlets are
127   located (Fig. 1A). The incision on the dura was covered with gel foam and the
128   laminectomy was closed with acrylic cement. A silver plate (3 × 2 mm) was used as a
129   reference electrode and placed on the T1 vertebra. The bundle of electrode wires
130   covered with silicon tubing was glued with dental acrylic to bone screws placed in the
131   T1 dorsal process and subcutaneously routed to the skull and its connector was mounted
132   with acrylic resin. The skin and back muscle incisions were sutured with silk or nylon
133   threads, respectively.

134   **2.2.3 Implantation of microwires on forelimb muscles**

135   Electromyography (EMG) wires were surgically implanted in the right arm and hand
136   muscles. The target muscles were identified by anatomical features and movements
137   evoked by trains of low-intensity electrical stimulation. Bipolar, multi-stranded
138   stainless-steel wires (AS631, Cooner Wire Company, Chatsworth, CA, USA) were
139   sutured into each muscle and routed subcutaneously to the skull, and their connectors
140   (MCP-12-SS; Omnetics, Minneapolis, MN, USA) were anchored to the skull. The EMG
141   electrodes were implanted in the following 11 muscles. Four digit muscles: flexor
142   digitorum superficialis (FDS), extensor digitorum communis (EDC), flexor digitorum

143 profundus (FDP), and extensor digitorum 4 and 5 (ED45); five wrist muscles: flexor
144 carpi radialis (FCR), palmaris longus (PL), flexor carpi ulnaris (FCU), extensor carpi
145 ulnaris (ECU), and extensor carpi radialis (ECR); and two elbow muscles: biceps
146 brachii (BB) and brachioradialis (BR).

147

148 **2.3 Outline of the corticospinal interface**

149 To regain volitional control of the paralyzed forearm, a corticospinal interface that
150 connected an arbitrarily selected neuron in M1 and a spinal site caudal to the SCI site
151 was used (Fig. 2). A two- or three-graded torque-tracking task was used to evaluate the
152 motor function of the right wrist. One experimental session consisted of three
153 experiments (Fig. 3A) as follows. To determine a peripheral target location for
154 voluntary torque control, the direction and magnitude of the evoked wrist torque was
155 confirmed first by applying current to an arbitrarily selected electrode on the cervical
156 enlargement while the monkeys were at rest (Figs. 1, 3B, "Spinal stimulation at rest").
157 Next, to investigate the firing pattern of M1 cells before applying the corticospinal
158 interface, data were obtained without the corticospinal interface (Fig. 3C, "Before
159 corticospinal interface trials"). Finally, the corticospinal interface was then connected
160 from an arbitrarily selected neuron in M1 to a spinal site located caudal to the SCI (Fig.
161 3D, "During corticospinal interface trials"). The corticospinal interface was designed to
162 detect the firing rate of an arbitrarily selected neuron and convert it in real time to
163 activity-contingent electrical stimulation of a spinal site located caudally to the SCI. To
164 verify that the monkeys could not acquire the peripheral target through volitional
165 muscle contractions, it was sometimes turned off during a catch trial ("Catch" in Fig.
166 3D, "During catch trials").

167 In total, both monkeys completed 63 sessions, using 11 different pairs of neurons in M1
168 and spinal sites (Table 1, Monkey E, N = 40 sessions [7 sessions included catch trials];
169 Monkey L, N = 23 sessions [1 session included catch trials]).

170 **2.3.1 Investigation of the relationship between spinal stimulation and motor output**

171 To determine the stimulus parameters for the corticospinal interface, "Spinal stimulation
172 at rest" tests were conducted at the beginning of each session (Fig. 3B). While the right
173 upper limb was fixed in an experimental apparatus recording two-dimensional wrist

174   isometric torque (Fig. 1A), subdural spinal stimuli consisting of 10 constant-current,

175   biphasic square-wave pulses (each pulse 0.2 ms in duration) were delivered at 40 Hz

176   through a single electrode using a stimulator (ULI-100; Unique Medical Corporation,

177   Tokyo, Japan) targeting an arbitrarily selected electrode on the cervical enlargement.

178   Stimulus trains were delivered 3–225 times with an interval of 2,000 ms (Fig. 1E, F).

179   The direction and magnitude of the evoked wrist torque was measured at a stimulus

180   intensity between 1.0–3.4 mA (Fig. 1D, G, H).

181   **2.3.2 Real-time corticospinal interface**

182   To achieve a corticospinal interface that sends voluntary commands to the preserved

183   spinal site by bypassing the spinal lesion, the firing rate of an arbitrarily selected neuron

184   (linked neuron) in M1 was converted into stimulus pulses, and electrical stimulation

185   was delivered through an arbitrarily selected electrode on the cervical enlargement. The

186   corticospinal interface was accomplished using a computer interface that was designed

187   to detect the action potentials of the linked neuron specifically using a template-

188   matching algorithm (Blackrock Microsystems, Salt Lake City, UT, USA) and convert

189   them in real time into a stimulus current and frequency that were dependent on the

190   firing rate of the linked M1 cell. The moving averaged firing rate (50-ms time window)

191   of the linked neuron had a proportional relationship with the stimulation current and

192   frequency; thus, the monkeys could voluntarily co-modulate the current and frequency

193   of the electrical stimuli by changing the firing rate of the linked neuron (Fig. 2A).

194   If the averaged firing rate of the linked neuron (X [Hz]) was above the stimulus

195   threshold (X_{th} [Hz]), the stimulus frequency (f [Hz]) and current (I [mA]) were

196   modulated by the following equations:

197
$$f = f_0 + \frac{f_{\text{g}}}{X_{\text{th}}} \cdot (X - X_{\text{th}}), (f_0 \leq f \leq f_{\text{Max}})$$

198   where f_0 = initial stimulus frequency when X [Hz] was above X_{th} [Hz], f_{g} = gain of the

199   stimulus frequency, f_{Max} = maximum stimulus frequency [Hz].

200
$$I = I_0 + \frac{I_{\text{g}}}{X_{\text{th}}} \cdot (X - X_{\text{th}}), (I_0 \leq I \leq I_{\text{Max}})$$

201   where I_0 = initial stimulus current, I_g = gain of the stimulus current, I_{Max} = maximum

202   stimulus current [mA].

203   In both monkeys, the stimulus parameters were determined based on the results

204   obtained in the testing periods "Spinal stimulation at rest" and "Before corticospinal

205   interface" as follow: X_{th}, 10–60 Hz; f_0, 30 Hz; f_g, 5 Hz; f_{Max}, 40 Hz; I_0, 1.10–3.10 mA; I_g,

206   0.02 mA; I_{Max}, 1.26–3.60 mA. Each parameter had to meet the following criteria: X_{th},

207   higher than the average firing rate of the linked neuron during the "Before corticospinal

208   interface" period; f_0 and I_0, the initial stimulus frequency and intensity that did not

209   allow the monkeys to reach the peripheral target (see 2.5 Behavioral task); f_g and I_g, the

210   gains of stimulus frequency and intensity that could induce a smooth movement

211   trajectory, respectively; f_{Max} and I_{Max}, the maximum stimulus frequency and intensity

212   that generated an overshoot of the peripheral targets (see Behavioral task).

213   The initial stimulus current (I_0), and maximum stimulus current (I_{Max}) were sometimes

214   adjusted to maintain a consistent relationship between wrist torque and the firing rate of

215   the linked neurons.

216

217   **2.4 Behavioral task**

218   Before SCI, each monkey was trained to control the position of a cursor on a video

219   monitor with isometric wrist torque (torque-tracking task) and to acquire targets

220   displayed on the screen as described elsewhere (Nishimura et al., 2013; Kato et al.,

221   2019; Kaneshige et al., 2022). In this task, the movement direction of the cursor on the

222   screen coincided with the direction of wrist torque (Fig. 3). Behavioral experiments

223   started after the monkey's performance reached 10 trials/min for 10 consecutive

224   sessions prior to SCI without the corticospinal interface. Trials were initiated by

225   entering the center target and holding for a period of 800 ms. The "Go" cue (appearance

226   of a peripheral target) was provided after the hold period. After SCI, the peripheral

227   target position was set on the way of the evoked torque trajectory confirmed in the

228   "Spinal stimulation at rest" testing period, so that the wrist torque required to hit the

229   target was set at 25–70% (gray circle in the bottom panels of Fig. 3) of the evoked peak

230   torque (red dot in the bottom panel of Fig. 3B). The "End" cue (appearance of a center

231   target) was provided after a peripheral hold period of 300–400 ms. A liquid reward was

232   provided after a successful reach to each target and a center hold period of 500 ms. The

233   monkeys were required to clear the hold criterion within 10 s. When the hold criterion

234   was met or the 10-s period was not achieved, the next target was presented, either

235   immediately or after a reward period (Inter-trial interval: 1 s). The monkeys participated

236   in a total of 63 torque-tracking task sessions with the corticospinal interface (Monkey E,

237   40 sessions; Monkey L, 23 sessions). In several sessions (Monkey E, 16/40 sessions;

238   Monkey L, 5/23 sessions), the monkeys performed a three-graded torque-tracking task

239   in which peripheral targets appeared at two different positions (i.e., different magnitudes

240   of wrist torque in the same direction were required to perform the task successfully). In

241   the three-graded torque-tracking task, trials in which a peripheral target was located

242   close to the center target ("Weak" torque trials) required the production of 60% of the

243   wrist torque required in trials in which a peripheral target was located farther from the

244   center target ("Strong" torque trials). The timing of when the cursor entered the

245   peripheral targets ("In") was defined as the last time the cursor entered the peripheral

246   target after the "Go" cue during a successful trial (Fig. 7).

247

248   **2.5 Data collection**

249   A 96-channel array was connected to a multi-channel amplifier. Neural signals were

250   recorded at a sampling rate of 30 kHz and a bandpass filter was applied at 250–

251   7,500 Hz. EMG signals were amplified using a multichannel amplifier (AB-611J; Nihon

252   Kohden, Tokyo, Japan) at a gain of ×100 and bandpass filtered at 50–3,000 Hz. EMG

253   signals, wrist torque (flexion-extension and ulnar-radial directions), task parameters

254   such as target positions, and the timing of trial events were recorded simultaneously

255   with the neural signal using a Cerebus multichannel data acquisition system (Blackrock

256   Microsystems, Salt Lake City, UT, USA) at a sampling rate of 10 kHz. All recorded

257   signals were down-sampled to 1 kHz for offline analysis.

258

259   **2.6 Data analysis**

260   **2.6.1 Evoked muscle activity and wrist torque**

10

261   To minimize the effect of artifact contamination by spinal electrical stimulation on
262   EMG recordings, the raw EMG data from 2 ms before to 2 ms after stimulus timing
263   were removed, and the remaining data were analyzed.

264   The stimulus- or spike-triggered averages of rectified EMG and wrist torque data were
265   compiled (Fig. 1F, 2B, C). The magnitude and angle of wrist torque were measured
266   when the average wrist torque induced by spinal stimulation reached the maximum
267   value (red dot in right panel of Fig. 1D). To investigate the relationship between the
268   current intensity of spinal stimulation and the magnitude of the evoked torque, Pearson
269   correlation coefficients were computed between them for each spinal site (Fig. 1H).

270   Mean baseline activity and standard deviation were measured from rectified EMG
271   traces in the period from 50 to 0 ms preceding the trigger pulse. The onset latency of
272   muscle activation or stimulation of the biggest response was detected as greater than 3
273   standard deviations from the mean baseline (Fig. 2B, C).

274   **2.6.2 Neuronal activity**

275   Spikes from single M1 units were sorted using the Offline Sorter software package
276   (Plexon, Dallas, TX, USA) by projecting waveforms into principal component space
277   and identifying isolated clusters, and spike timings were smoothed (window: 200 ms)
278   and down-sampled from 30 kHz to 1 kHz for offline analysis. Neuronal activity was
279   analyzed separately in neurons linked to spinal stimulation (linked neurons) and others
280   (unlinked neurons). For a fair comparison between before and during the corticospinal
281   interface condition, data from the same number of trials (9–55 trials) before and during
282   the corticospinal interface condition were analyzed. Data during the corticospinal
283   interface condition were extracted from a peak performance period in the first 10 min.
284   The data in the catch trials were extracted from the entire corticospinal interface
285   condition.

286   Unlinked neurons were classified into task-related neurons and task-unrelated neurons
287   ("unrelated neurons") as follows. The average firing rate of each neuron was calculated
288   in a 400-ms period around two task events: before the Go cue (Figs. 5A, 7A: -500 to -
289   100 ms relative to peripheral target appearance) and after the Go cue (Fig. 5A: 100 to
290   500 ms relative to peripheral target appearance, Fig. 7A: -200 to 200 ms relative to the
291   timing of "In"). A neuron was defined as "task-related" if there was a significant

292   difference in its average firing rate between before and after the Go cue. Then, the task-
293   related neurons were classified into "increased neurons" and "decreased neurons" as
294   follows. An increased neuron was defined by a significant increase of its firing rate after
295   the Go cue relative to before the Go cue, and a decreased neuron was defined by a
296   significant decrease of its firing rate after the Go cue relative to before the Go cue (Figs.
297   5A, 7A).

298   To examine changes in the activity of unlinked neurons in representative sessions (Figs.
299   5A, 7A), the firing rates of the unlinked neurons were z-scored using the firing rates
300   during a 400-ms period (500–100 ms before the Go cue).

2.6.3 Task-related modulation

302   To examine the changes of activity before and after peripheral target appearance, the
303   modulation depths (MDs) of neural activity, EMG, and torque were calculated. MD was
304   defined as the difference in the average firing rate of M1 cells, rectified EMG, and wrist
305   torque between before the Go cue (Figs. 5A, 7A: -500 to -100 ms relative to peripheral
306   target appearance) and after the Go cue (Fig. 5A: 100 to 500 ms relative to peripheral
307   target appearance; Fig. 7A: -200 to 200 ms relative to the timing of "In") in each
308   session.

2.6.4 Task performance

310   Task performance was defined as the maximum number of successful trials/min in each
311   condition.

2.6.5 Statistical analysis

313   To determine whether there were statistically significant differences in the MDs of the
314   firing rate of M1 cells, rectified EMG, wrist torque, and task performance before and
315   during the corticospinal interface (two- and three-graded tasks) and during the catch
316   trials (Figs. 4B–E, 6A–I, 7B–E, 8A–I), a paired *t*-test with Bonferroni's correction was
317   performed.

318   To determine whether there were statistically significant differences in the MDs of the
319   firing rate of the linked and unlinked neurons before and during the corticospinal

320   interface (two- and three-graded tasks) and during the catch trials (Fig. 9), the Wilcoxon

321   rank-sum test was performed.

322   The classification of unlinked neurons into "task-related neurons", "task-unrelated

323   neurons", "increased neurons" and "decreased neurons" was based on the P-value of a

324   paired *t*-test.

325   To compare the percentages of the type of unlinked neurons before and during the

326   corticospinal interface and between the weak and strong torque trials, a chi-squared test

327   was used (Figs. 5B, 7F).

328   Statistical significance was considered at $P < 0.05$, unless otherwise noted.

329   All statistical analyses were performed with MATLAB 2014a and 2021a statistical tool

330   box (MathWorks, Inc., Natick, MA, USA) and R (version 4.1.1; R Foundation for

331   Statistical Computing, Vienna, Austria).

332

333   **2.7 Confirmation of lesion extent**

334   At the end of all experiments, the monkeys were anesthetized deeply with an overdose

335   of sodium pentobarbital (50 mg/kg, i.v.) and perfused transcardially with 0.1 M

336   phosphate-buffered saline (pH 7.4), followed by 10% formaldehyde in 0.1 M phosphate

337   buffer (pH 7.4). The perfused spinal cord was removed and immersed successively in

338   10%, 20%, and 30% sucrose in 0.1 M phosphate buffer (pH 7.3). The specimens were

339   cut serially into coronal sections of 50-µm thickness on a freezing microtome, and every

340   5th section was mounted on a gelatin-coated glass slide and Nissl-stained with 0.5%

341   cresyl violet. Photomicrographs of the spinal cord lesion were captured. The extent of

342   the lesion was defined by the area of gliosis.

343   **3 Results**

344   **3.1 A primate spinal lesion model**

345   Two macaque monkeys were subjected to unilateral SCI that was limited to the border

346   between the C4 and C5 segments on the right side (Fig. 1A, B). The lesion was

347   extended into the lateral funiculus and dorsal column including a substantial portion of

348   the descending and ascending pathways (Fig. 1B). Immediately after lesioning, Monkey

349   E displayed hemiplegia on the ipsilesional side. No apparent movement of the forearms,

350   including the finger and wrist joints, was observed, but there was weak muscle activity

351   at the elbow and shoulder joints on the ipsilesional side. The lower extremity showed a

352   nearly complete motor deficit on the ipsilesional side. Monkey L displayed a nearly

353   complete motor deficit of the upper and lower extremities on both sides. Since the

354   animals did not respond to noxious mechanical stimulation of body parts on the lesioned

355   side, somatosensory functions appeared to be impaired on the lesioned side in both

356   animals. Experiments in Monkeys E and L were performed until post-SCI day 45 and

357   33, respectively. Neither animal showed an improvement of the voluntary control of the

358   fingers and wrist joint throughout the experimental period.

359

360   **3.2 Evoked wrist torque by subdural spinal stimulation during rest**

361   To confirm the effect of subdural spinal stimulation on muscle activity of the forearm

362   and wrist torque, tonic spinal stimuli were delivered at various current intensities from

363   an electrode on the cervical enlargement (C6–T1) in two monkeys with SCI. Subdural

364   spinal stimuli consisting of 10 constant-currents at 40 Hz were delivered through a

365   single electrode while the monkeys were not required to produce any wrist torque to

366   hold a cursor in a resting position of a center target (Fig. 1). Figure 1D–F shows typical

367   examples of the wrist torque and EMG responses induced by subdural spinal

368   stimulation of C8 at 1.8 mA (electrode no. 5, Monkey E, post-SCI day 14). Spinal

369   stimulation induced responses in multiple muscles and wrist torque (Fig. 1E, F). The

370   magnitude and direction of the evoked torque were 0.27 kg/cm^{-1} and ulnar-flexion

371   (218°, right panel in Fig. 1D), respectively. Figure 1G shows the population data for the

372   direction of the evoked torque. Tonic spinal stimuli at various current intensities

373   (Monkey E, 1.2–3.4 mA; Monkey L, 1.0–2.2 mA) at the caudal region of the cervical

14

374 enlargement (black circles in the top panels of Fig. 1G) induced wrist torque in the

375 direction of flexion to ulnar-flexion (Monkey E, 179–243°; Monkey L, 193–260°). The

376 magnitude of the evoked torque was positively correlated with current intensity (Fig.

377 1H, Monkey E: electrode 4 [red], R = 0.53, P = 1.08×10^{-2}; electrode 5 [blue], R = 0.49,

378 P = 9.81×10^{-3}; electrode 6 [black], R = 0.53, P = 1.74×10^{-3}; Monkey L: electrode 5

379 [blue], R = 0.47, P = 3.07×10^{-5}; electrode 6 [black], R = 0.92, P = 1.42×10^{-8}). These

380 results demonstrated that subdural spinal stimulation of the preserved cervical

381 enlargement induced the activation of multiple forearm muscles and wrist torque of the

382 paralyzed forearm in the range from flexion to ulnar-flexion. We also found that the

383 magnitude of the evoked torque could be controlled by changing current intensity.

384

385 **3.3 Volitional control of the paralyzed forearm via a corticospinal interface**

386 To regain volitional control of the paralyzed forearm, we employed a corticospinal

387 interface that connected an arbitrarily selected neuron in M1 (linked neuron) and a

388 spinal site for bridging the SCI site. The firing rate of an arbitrarily selected linked

389 neuron was converted into stimulus pulses, and electrical stimulation was delivered

390 through an arbitrarily selected electrode on the cervical enlargement (Fig. 2A). Figure

391 2B shows the latencies of spinal stimulation and muscle activation from the action

392 potentials of a linked neuron. The average latency of spinal stimulation was 47.2 ± 15.9

393 ms (Fig. 2D, 363–19,258 spikes in 62 sessions during the corticospinal interface trials

394 [Monkey E, N = 2,694–19,258 spikes; Monkey L, N = 363–12,461 spikes], Monkey E,

395 54.0 ± 0 ms; Monkey L, 42.7 ± 30.9 ms). The average latency of evoked muscle activity

396 was 53.0 ± 16.6 ms (Fig. 2D, Monkey E, 59.8 ± 2.83 ms; Monkey L, 43.8 ± 24.3 ms).

397 The latencies of muscle activation in proximal muscles such as the BB and BR were

398 similar to those of distal muscles such as the EDC, ED45, and FDS (Fig. 2D, PL, ECU

399 and ECR: N = 62, FDS: N = 24, FDP and EDC: N = 61, ED45: N = 2, BR: N = 40,

400 others: N = 63 [Monkey E, FDS and ED45: N = 2, FDP and EDC: N = 38, others: N =

401 40; Monkey L, PL, FDS, ECU and ECR: N = 22, ED45 and BR: N = 0, others: N =

402 23]).

403 We also investigated the latency of muscle activation from spinal stimulation (Fig. 2C).

404 The average latency of muscle activation from spinal stimulation was 4.10 ± 1.35 ms

405 (Fig. 2E, 345–13,130 spikes in 63 sessions during the corticospinal interface trials

406   [Monkey E, N = 1,956–13,130 spikes; Monkey L, N = 345–9,753 spikes], Monkey E,

407   4.98 ± 0.77 ms; Monkey L, 5.31 ± 1.97 ms). The latencies of muscle activation in

408   proximal muscles were similar to those of distal muscles (Fig. 2E, FDS: N = 25, FDP

409   and EDC: N = 61, ED45: N = 2, BR: N = 40, others: N = 63 [Monkey E, FDS and

410   ED45: N = 2, FDP and EDC: N = 38, others: N = 40; Monkey L, ED45 and BR: N = 0,

411   others: N = 23]).

412   To determine a peripheral target location for voluntary torque control, the direction and

413   magnitude of evoked wrist torque were confirmed by injecting current to an arbitrarily

414   selected spinal site while the monkeys were at rest. The representative example in

415   Figure 3B shows the trajectory of wrist torque induced by subdural electrical

416   stimulation of C8 at 1.8 mA. The peripheral target location was set on the evoked

417   trajectory and at half the maximum torque value induced by the tested current (gray

418   circle in the bottom panels in Fig. 3B–D). Therefore, the monkeys were required to

419   regulate the torque output of the paralyzed forearm by modulating the firing rate of the

420   linked neuron that controls the current and frequency of spinal stimulation to acquire the

421   target.

422   To investigate the firing pattern of M1 cells before applying the corticospinal interface,

423   data were obtained in its absence. The firing patterns of most M1 neurons, forelimb

424   muscle activity, and wrist torque showed no apparent changes related to the task

425   requirements (Fig. 3C).

426   The corticospinal interface was then connected from a linked neuron to a spinal site

427   located caudally to the SCI. The corticospinal interface was designed to detect the firing

428   rate of an arbitrarily selected "linked neuron" and convert it in real time to activity-

429   contingent electrical stimulation to a spinal site located caudally to the SCI. The current

430   intensity and frequency applied to the spinal site were proportional to the firing rate of

431   the linked neuron. The monkeys could regulate the current intensity and frequency of

432   the electrical stimulation by altering the firing rate of the linked neuron (Fig. 3D); thus,

433   they could control the activity of the paralyzed wrist muscles and the magnitude of wrist

434   torque, leading to repeated target acquisition. To confirm the feasibility of the

435   corticospinal interface, it was turned off during catch trials ("Catch" in Fig. 3D). During

436   the catch trials, the monkeys continued to increase the firing rate of the linked neuron;

437   however, they were unable to acquire the peripheral target due to paralysis, indicating

438   that the corticospinal interface was necessary for the voluntary control of wrist torque.

439   To investigate how monkeys with SCI utilized the corticospinal interface, we

440   investigated the activity of linked neurons and paralyzed muscles and wrist torque.

441   Figure 4A shows a typical example of the firing pattern of a linked neuron, muscle

442   activity, and wrist torque before and during the corticospinal interface and during the

443   catch trials (Monkey E, post-SCI day 15, electrode: 5, I_0: 1.7 mA, I_{Max}: 1.8 mA, I_g: 0.01

444   mA, f_0: 30 Hz, f_{Max}: 40 Hz, f_g: 5 Hz, pulse width: 0.2 ms). The firing rate of the linked

445   neuron did not show remarkable modulation before the corticospinal interface trials (left

446   panel in Fig. 4A), while it showed task-related modulation that increased after

447   peripheral target appearance during the corticospinal interface and catch trials (center

448   and right panels in Fig. 4A). The frequency of spinal stimulation, EMG, and wrist

449   torque were also co-modulated with the firing rate of the linked neuron during the

450   corticospinal interface trials (center panels in Fig. 4A), whereas negligible muscle

451   activity and no apparent wrist torque were produced before the corticospinal interface

452   and during the catch trials (left and right panels in Fig. 4A). The MDs of the linked

453   neurons during the corticospinal interface and catch trials were significantly increased

454   compared to before the corticospinal interface trials (Fig. 4B, paired t-test with

455   Bonferroni's correction: P $_{before\ vs.\ during}$ = 6.53×10^{-18}, P $_{before\ vs.\ during\ catch\ trials}$ = $3.45 \times 10^{-}$

456   ^{4}). Similarly, the MDs of EMG (Fig. 4C) and torque (Fig. 4D) during the corticospinal

457   interface trials were also significantly increased compared to before the corticospinal

458   interface trials (Fig. 4C, paired t-test with Bonferroni's correction: P $_{before\ vs.\ during}$ = 5.67

459    $\times 10^{-62}$; Fig. 4D, paired t-test with Bonferroni's correction: P $_{before\ vs.\ during}$ = 2.38×10^{-15}).

460   However, the MDs of EMG (Fig. 4C) and torque (Fig. 4D) during the catch trials were

461   significantly decreased compared to during the corticospinal interface trials (Fig. 4C,

462   paired t-test with Bonferroni's correction: P $_{during\ vs.\ during\ catch\ trials}$ = 3.69×10^{-21}; Fig. 4D,

463   paired t-test with Bonferroni's correction: P $_{during\ vs.\ during\ catch\ trials}$ = 1.45×10^{-4}) due to the

464   absence of spinal stimulation, and the monkeys failed to acquire the peripheral target

465   (Fig. 3D, right panel in Fig. 4E).

466   In total, both monkeys performed the experiments in 63 sessions, using 11 different

467   pairs of neurons in M1 and spinal sites (Table 1, Monkey E, N = 40 sessions [catch: 7

468   sessions of those included in the catch trials]; Monkey L, N = 23 sessions [catch: 1

469   session of those included in the catch trials). The monkeys reached peak performance at

470   6.19 ± 2.99 min (Monkey E, 7.15 ± 2.69 min; Monkey L, 4.52 ± 2.78 min) in the first

471   10 min during the corticospinal interface. The average peak task performance was

472   significantly lower with the corticospinal interface after SCI (11.70 ± 5.31 trials/min,

473 [Monkey E, 13.18 ± 4.73 trials/min, N = 40 sessions; Monkey L, 10.23 ± 5.82

474 trials/min, N = 23 sessions]) than without the corticospinal interface before SCI (19.34

475 ± 1.63 trials/min, [Monkey E, 17.78 ± 0.29 trials/min, N = 10 sessions; Monkey L,

476 20.91 ± 0.25 trials/min, N = 10 sessions], unpaired t-test: P $_{\text{before SCI vs. after SCI}}$ = 5.52 × 10$^-$

477 ^{8}), but was significantly higher than before the corticospinal interface and during the

478 catch trials after SCI (Fig. 4E, paired t-test with Bonferroni's correction: P $_{\text{before vs. during}}$ =

479 1.94 × 10^{-26}, P $_{\text{before vs. catch trials}}$ = 0.321, P $_{\text{during vs. catch trials}}$ = 2.67 × 10^{-26}). These results

480 suggest that the corticospinal interface was essential for the voluntary control of the

481 wrist torque of the paralyzed forearm.

482

483 **3.4 Task-related modulation of unlinked neurons during the corticospinal interface**

484 Since we used a multi-channel electrode array, which enabled the recording of

485 assemblies of M1 neurons, we investigated how unlinked neurons, which were not

486 connected to the interface, modulated their activity in response to the corticospinal

487 interface. Figure 5A shows a typical example of the task-related modulation of linked

488 and unlinked neurons before and during the corticospinal interface and during the catch

489 trials (Monkey E, post-SCI day 15, Electrode: 5, I_0: 1.7 mA, I_{Max}: 1.8 mA, I_{g}: 0.01 mA,

490 f_0: 30 Hz, f_{Max}: 40 Hz, f_{g}: 5 Hz, pulse width: 0.2 ms). Before the corticospinal interface

491 trials, most of the unlinked neurons did not show task-related modulation of their

492 activity, as for a linked neuron (left panel in Fig. 5A). Conversely, during the

493 corticospinal interface trials, many unlinked neurons exhibited task-related modulation

494 of their activity. We found two types of unlinked neurons exhibiting task-related

495 activity: neurons that increased their firing rate and neurons that decreased their firing

496 rate in response to the required torque (center panel in Fig. 5A). During the catch trials,

497 task-related modulation in the unlinked neurons was similar to the activity during the

498 corticospinal interface trials. Although spinal stimulation was not applied in the catch

499 trials, only the proximal arm muscles showed small changes in their activity. However,

500 the wrist muscles did not show any activity, so the monkeys failed to generate wrist

501 torque (right panel in Fig. 5A).

502 To characterize the change in the activity of the unlinked neurons, they were classified

503 into "task-related" and "task-unrelated" neurons (unrelated neurons, middle panels of

504 the heatmap in Fig. 5A) (see Methods). The task-related neurons were further classified

505   into "increased" (top panels of the heatmap in Fig. 5A) neurons and "decreased"

506   (bottom panels of the heatmap in Fig. 5A) neurons, which showed increased and

507   decreased activity in response to the task, respectively (Fig. 5). Although the majority

508   were "task-unrelated" unlinked neurons before the corticospinal interface trials, the

509   percentage of "task-unrelated" unlinked neurons decreased during the corticospinal

510   interface and catch trials, indicating that the firing pattern of "task-unrelated" unlinked

511   neurons changed to that of "task-related" neurons (Fig. 5B, 3,961 neurons in 63 sessions

512   before and during corticospinal interface trials [Monkey E, N = 1,846 neurons; Monkey

513   L, N = 2,115 neurons], 414 neurons in eight sessions in catch trials [Monkey E, N = 312

514   neurons; Monkey L, N = 102 neurons], chi-squared test: χ^2 = 593.15, P = 4.70 × 10^{-127}]).

515   In addition, the MDs of neuronal firing in the "increased" (Fig. 6A, paired t-test with

516   Bonferroni's correction: $P_{\text{before vs. during}}$ = 1.39 × 10^{-10}, $P_{\text{before vs. during catch trials}}$ = 1.54 × 10^{-1},

517    $P_{\text{during vs. during catch trials}}$ = 3.21 × 10^{-1}; Fig. 6B, paired t-test with Bonferroni's correction: P

518    $_{\text{before vs. during}}$ = 6.17 × 10^{-81}, $P_{\text{before vs. during catch trials}}$ = 2.47 × 10^{-2}, $P_{\text{during vs. during catch trials}}$ =

519   2.11 × 10^{-3}; Fig. 6C, paired t-test with Bonferroni's correction: $P_{\text{before vs. during}}$ = 1.31 ×

520   10^{-19}, $P_{\text{before vs. during catch trials}}$ = 1.52 × 10^{-4}, $P_{\text{during vs. during catch trials}}$ = 4.33 × 10^{-1}) and

521   "decreased" (Fig. 6G, paired t-test with Bonferroni's correction: $P_{\text{before vs. during}}$ = 3.27 ×

522   10^{-14}, $P_{\text{before vs. during catch trials}}$ = 1.16 × 10^{-1}, $P_{\text{during vs. during catch trials}}$ = 2.23 × 10^{-1}; Fig. 6H,

523   paired t-test with Bonferroni's correction: $P_{\text{before vs. during}}$ = 3.67 × 10^{-133}, $P_{\text{before vs. during}}$

524    $_{\text{catch trial}}$ = 3.46 × 10^{-7}, $P_{\text{during vs. during catch trials}}$ = 4.16 × 10^{-8}; Fig. 6I, paired t-test with

525   Bonferroni's correction: $P_{\text{before vs. during}}$ = 8.25 × 10^{-17}, $P_{\text{before vs. during catch trials}}$ = 3.12 × 10^{-}

526   ^{2}, $P_{\text{during vs. during catch trials}}$ = 5.83 × 10^{-1}) neurons were greater during the corticospinal

527   interface trials than before them. Conversely, "unrelated" neurons during the

528   corticospinal interface trials showed a smaller change of the MDs or maintained their

529   characteristics in different trial types (Fig. 6D, paired t-test with Bonferroni's

530   correction: $P_{\text{before vs. during}}$ = 5.04 × 10^{-19}, $P_{\text{before vs. during catch trials}}$ = 1.44 × 10^{-1}, $P_{\text{during vs.}}$

531    $_{\text{during catch trials}}$ = 9.39 × 10^{-1}; Fig. 6E, paired t-test with Bonferroni's correction: $P_{\text{before vs.}}$

532    $_{\text{during}}$ = 9.74 × 10^{-1}, $P_{\text{before vs. during catch trials}}$ = 2.19 × 10^{-2}, $P_{\text{during vs. during catch trials}}$ = 3.42 × 10^{-}

533   ^{1}; Fig. 6F, paired t-test with Bonferroni's correction: $P_{\text{before vs. during}}$ = 7.29 × 10^{-27}, P_{before}

534    $_{\text{vs. during catch trials}}$ = 2.44 × 10^{-4}, $P_{\text{during vs. during catch trials}}$ = 6.20 × 10^{-1}). Thus, a subgroup of

535   "unlinked" neurons also responded to the corticospinal interface as well as "linked"

536   neurons. Conversely, the MDs during the catch trials tended to be smaller than those

537   during the corticospinal interface trials (Catch in Figs. 5A, 6B, 6H).

538

539   **3.5 Modulation of the torque of the paralyzed hand via a corticospinal interface**

540   The results demonstrated that the linked neurons showed task-related modulation via the
541   corticospinal interface, and this modulation contributed to success in the torque-tracking
542   task. However, it was not clear whether this modulation was caused by the monkeys
543   simply aiming for a certain firing rate of a linked neuron or if they understood the
544   relationship between the evoked torque and the target and modulated the firing rate of a
545   linked neuron as needed. To investigate whether the monkeys recognized this
546   relationship, we conducted a three-graded torque-tracking task by setting targets that
547   required the monkeys to generate "Weak" torque, "Strong" torque, or no torque. Figure
548   7A illustrates a typical example of neuronal activity, EMG, and wrist torque when
549   targets requiring "Weak" and "Strong" torque were presented. The monkeys
550   successfully completed the task by adjusting wrist torque to the required amount for
551   each target (Monkey E, post-SCI day 16, Electrode: 5, I_0: 1.7 mA, I_{Max}: 1.8 mA, I_g: 0.01
552   mA, f_0: 30 Hz, f_{Max}: 40 Hz, f_g: 5 Hz, pulse width: 0.2 ms). The linked neurons varied
553   their firing rates according to the required magnitude of wrist torque. The MDs of the
554   linked neurons in the "Strong" torque trials were significantly greater than those of the
555   "Weak" torque trials (Fig. 7B, paired *t*-test: P = 1.04×10^{-11}), and the MDs of EMG and
556   torque in the "Strong" torque trials were also significantly greater than those of the
557   "Weak" torque trials (EMG in Fig. 7C, paired *t*-test: P = 1.26×10^{-46}; wrist torque in
558   Fig. 7D, paired *t*-test: P = 6.39×10^{-10}). There was no significant difference in task
559   performance between the "Weak" and "Strong" torque trials (Fig. 7E, paired *t*-test with
560   Bonferroni's correction: P $_{before\ vs.\ in\ weak\ torque\ trials}$ = 5.36×10^{-16}, P $_{before\ vs.\ in\ strong\ torque\ trials}$ =
561   2.33×10^{-16}, P $_{in\ weak\ torque\ trials\ vs.\ in\ strong\ torque\ trials}$ = 5.05×10^{-2}, P $_{in\ weak\ torque\ trials\ vs.\ during\ catch}$
562    $_{trials}$ = 5.36×10^{-16}, P $_{in\ strong\ torque\ trials\ vs.\ during\ catch\ trials}$ = 2.33×10^{-16}, P $_{before\ vs.\ during\ catch\ trials}$ =
563   1). Thus, monkeys with SCI were able to grade wrist torque voluntarily via the
564   corticospinal interface, suggesting that they understood the relationship between the
565   amount of evoked torque required to control the cursor and the target location and
566   modulated the firing rate of linked neurons as needed.

567   The firing rates of a subgroup of unlinked neurons were modulated in the same manner
568   as the linked neurons depending on the required magnitude of wrist torque (Fig. 7A). To
569   investigate whether the unlinked neurons changed their characteristics according to the
570   required torque, the percentage of characteristic combinations ("increased,"
571   "decreased," or "unrelated") in the "Weak" and "Strong" torque trials was calculated

572   (Fig. 7F, total in both monkeys: 21 sessions [Monkey E, N = 16 sessions; Monkey L, N

573   = 5 sessions], 1,284 neurons [Monkey E, N = 768 neurons; Monkey L, N = 516

574   neurons]). The majority of neurons maintained their characteristics at different torques,

575   although the percentage of "task-unrelated" unlinked neurons was decreased in the

576   strong trials, indicating that some "task-unrelated" unlinked neurons changed their

577   firing characteristics to "task-related" neurons with either "increased" or "decreased"

578   characteristics (Fig. 7F, chi-squared test: $\chi^2 = 14.381$, $P = 7.54 \times 10^{-4}$).

579   To clarify the possibility that even if neurons maintained their characteristics

580   ("increased" or "decreased"), they changed their MDs, we compared the MDs of the

581   unlinked neurons between the "Weak" and "Strong" torque trials (Fig. 8). Neurons that

582   consistently showed "increased" (Fig. 8A, paired t-test: $P = 4.41 \times 10^{-10}$), "unrelated"

583   (Fig. 8E, paired t-test: $P = 9.56 \times 10^{-3}$), and "decreased" (Fig. 8I, paired t-test: $P = 1.06$

584    $\times 10^{-13}$) characteristics in the "Weak" and "Strong" torque trials had significantly greater

585   MDs in the "Strong" torque trials than in the "Weak" torque trials. Thus, the unlinked

586   neurons also modulated their activity depending on the required magnitude of wrist

587   torque.

588

589   **3.6 Difference in modulation between linked and unlinked neurons**

590   We selected an arbitrary linked neuron from among an ensemble of M1 neurons.

591   However, it was unclear whether they had similar properties as unlinked neurons. To

592   investigate selection bias, we compared the MDs of linked and unlinked neurons before

593   and during the corticospinal interface and during catch trials. There was no difference in

594   the MDs between the linked and unlinked neurons before the corticospinal interface

595   (Fig. 9A, Wilcoxon rank-sum test: $P = 9.75 \times 10^{-2}$; Fig. 9D, Wilcoxon rank-sum test: $P =$

596   6.84×10^{-1}). The results indicate that the selection of neurons was unbiased. However,

597   during the corticospinal interface and catch trials, there were significant differences

598   between the MDs of linked and unlinked neurons (During corticospinal interface, Fig.

599   9B, Wilcoxon rank-sum test: $P = 5.03 \times 10^{-30}$; During catch trials, Fig. 9C, Wilcoxon

600   rank-sum test: $P = 4.35 \times 10^{-6}$). These results were also significantly different in the

601   weak and strong trials (Weak, Fig. 9E, Wilcoxon rank-sum test: $P = 4.53 \times 10^{-15}$; Strong,

602   Fig. 9F, Wilcoxon rank-sum test: $P = 4.15 \times 10^{-15}$).

21

603 **4 Discussion**

604 The aim of this study was to investigate the feasibility of a corticospinal interface for

605 the graded control of wrist torque of a paralyzed hand in monkeys with SCI at C4/C5.

606 The current intensity of subdural spinal stimulation on the preserved cervical

607 enlargement could modulate the magnitude of activation of paralyzed forearm muscles

608 and wrist torque. To send voluntary commands to the preserved spinal site by bypassing

609 the spinal lesion, we employed a corticospinal interface that connected an arbitrarily

610 selected neuron in M1 and a spinal site. The corticospinal interface modulated the

611 current intensity and frequency of spinal cord stimulation in proportion to the firing rate

612 of the linked neuron. Paralyzed monkeys were able to modulate torque output at the

613 wrist joint by modulating the firing rate of M1 neurons via the corticospinal interface,

614 indicating that the interface compensated for the function of the lesioned corticospinal

615 tract.

616

617 **4.1 Current intensity controls the magnitude of torque output, but not its direction**

618 Intact animals chiefly employ ordered motor unit recruitment and rate coding to

619 modulate muscle force output. As the level of contraction increases, additional motor

620 units are recruited, and the firing rates of motor units increase (Adrian and Bronk,

621 1929). Our results showed that the magnitude of the evoked wrist torque changed

622 according to the stimulus current and was positively correlated with current intensity

623 (Fig. 1H), indicating that current change was associated with the number and firing rate

624 of the recruited motor units. Furthermore, as we applied repetitive stimulation at 40 Hz

625 (as shown in Fig. 1F), temporal summation of the membrane potential of spinal neurons

626 and the resulting torque output also contributed to the production of stronger torque.

627 These types of temporal and spatial summation mechanisms play a role in modulating

628 torque output.

629 Since the subdural array covered the dorsal-lateral aspect of the cervical enlargement

630 beneath the dorsal root and dorsolateral funiculus (Fig. 1B), which contains

631 corticospinal and rubrospinal tracts, electrical currents are likely to first drive the

632 afferent fibers adjacent to the stimulation site, indicating that a major component of the

633 stimulus effect could be driven by the spinal reflex via large-diameter and low-threshold

634   afferent fibers. As stimulus current increases, it might drive the intersegmental spinal
635   circuitry and evoke the activation of multiple joints in the upper limb. In addition,
636   stimulation might activate descending tracts located in the dorsolateral funiculus, such
637   as the corticospinal and rubrospinal tracts, directly innervating the spinal circuits in the
638   cervical enlargement. Further higher currents, which induced a larger magnitude of
639   wrist torque, might spread to the ventral aspect of the spinal cord and lead to the direct
640   activation of motor axons. Thus, increasing current of subdural spinal stimulation
641   supposedly permits gradually recruitment of smaller to larger motoneurons, which in
642   turn, achieves gradient control of torque output.

643   Motor output from spinal stimulation has been examined extensively in anaesthetized
644   conditions, showing only excitatory effects for epidural spinal stimulation (Greiner et
645   al., 2021) and intraspinal microstimulation (Saigal et al., 2004; Moritz et al., 2007;
646   Zimmermann et al., 2011). In awake animals, spinal stimulation induces excitatory
647   and/or inhibitory effects on muscle activity during voluntary movements (Nishimura et
648   al., 2013; Kato et al., 2020; Kaneshige et al., 2022). The magnitude of this activation
649   depends on stimulation intensity (Kato et al., 2020; Kaneshige et al., 2022). However,
650   the effect of current intensity on motor output from spinal stimulation in awake injured
651   animals is unknown. Our results from awake monkeys with SCI showed that inhibitory
652   effects were unobservable due to the lack of background activity of the paralyzed
653   forearm muscles. However, subdural spinal cord stimulation induced muscle activity in
654   the paralyzed forearm (Fig. 1E, F). These results indicate that the excitability of the
655   spinal motoneuron pool is too low to observe the effect of inhibitory spinal interneurons
656   on motor output. This result was consistent with those obtained under anaesthetized
657   conditions in previous studies (Kato et al., 2020), indicating that the excitability of
658   spinal motoneurons in SCI is quite low due to the lack of descending inputs.

659   In daily life, we are required to control movements in a variety of directions, but
660   unfortunately, the present results in SCI animals with paralyzed forearm showed that
661   spinal stimulation of C7–T1 at rest could only induce torque in a limited range of
662   directions. Spinal stimulation at rest activated multiple muscles including flexor,
663   extensor, ulnar, and radial muscles about the wrist joint, while the directions of the
664   evoked torque responses were limited in the ulnar-flexion direction, irrespective of
665   current intensity (Fig. 1G). This result corresponds with our previous study
666   demonstrating that subdural spinal stimulation at higher currents evokes stereotypical

667   torque responses in the ulnar-flexion direction during voluntary torque production

668   (Kaneshige et al., 2022). This finding might be due to the large proportion of spinal

669   interneurons affecting flexor muscles (Perlmutter et al., 1998), a biomechanical

670   interaction between bones, ligaments, and musculotendon units for forearm movements

671   (Razavian et al., 2022), and the fact that the number and volume of wrist flexor and

672   ulnar muscles are greater than those of antagonist muscles (wrist radial and extensor

673   muscles), so that the evoked torque is limited in the ulnar-flexion direction.

674   **4.2 Voluntarily-controlled motor output through the corticospinal interface**

675   As mentioned above, voluntary contraction of skeletal muscles is controlled by two

676   mechanisms: one changes the number of active motor units and the other changes the

677   firing rate of individual motor units. Both mechanisms are regulated by commands from

678   descending pathways including the corticospinal neurons in the motor cortex. One is the

679   number of active descending neurons and the other is the firing rate of the activated

680   descending neurons. The corticospinal interface in the present study was designed to

681   emulate these processes and the anatomical connections of the corticospinal tract. The

682   interface was programmed to utilize the firing rate of a single M1 neuron and convert it

683   in real time to activity-contingent electrical stimulation of a spinal site. The stimulation

684   current and frequency applied to a spinal site were proportional to the firing rate of a

685   single neuron (Figs. 2A, 3D). In the corticospinal interface, modulation of the

686   stimulation current and frequency by a linked neuron is assumed to alter the number and

687   firing rate of corticospinal neurons which associate with the linked neuron, respectively.

688   The increased current might increase the excitability of the spinal circuits that recruit

689   more spinal motoneurons, as well as increase the firing rate of active motoneurons. The

690   increased frequency may also increase the excitability of the spinal circuits via temporal

691   and special summation of membrane potentials in spinal neurons, thus facilitating

692   recruitment and the rate-coding process. As a result, the task-related activity of the

693   linked neurons in M1 modulated the magnitude of the evoked torque and the activation

694   of multiple muscles depending on the required magnitude of wrist torque (Figs. 4, 5, 7).

695   Descending commands generated in the motor cortex for controlling voluntary limb

696   movements activate spinal motoneurons and interneurons. The functional loss of limb

697   control in individuals with SCI or stroke can be caused by the interruption of

698   corticospinal pathways originating from the motor cortex, although the neural circuits

699   located above and below the lesion remain functional. A substantial portion of

24

700   corticospinal pathways are derived from M1 (Toyoshima and Sakai, 1982; He et al.,

701   1993; Usuda et al., 2022). Numerous studies have shown that the neural activity in M1

702   represents the level of muscle activity (Fetz and Cheney, 1980; Cheney et al., 1985;

703   Buys et al., 1986; Lemon et al., 1986), joint torque (Evarts, 1968; Kakei et al., 1999),

704   and force (Cheney and Fetz, 1980; Sergio and Kalaska, 2003). Thus, M1 is the most

705   appropriate cortical source of the input signal controlling stimulation to the preserved

706   spinal cord for the control of muscle activation and joint torque. Indeed, the activity of a

707   single neuron (Moritz et al., 2008; Zimmermann and Jackson, 2014) or an ensemble of

708   neurons (Pohlmeyer et al., 2009; Ethier et al., 2012; Nishimura et al., 2013; Bouton et

709   al., 2016; Ajiboye et al., 2017; Kato et al., 2019; Barra et al., 2022) in M1 can be used

710   as a signal to control the stimulation parameters to determine the contraction level of

711   paralyzed muscles. The motor cortex contains corticospinal neurons that project directly

712   to the spinal cord and neurons that project to other subcortical nuclei or the cerebral

713   cortex. A corticospinal neuron controls the activity of multiple target muscles (Fetz and

714   Cheney, 1979; Cheney et al., 1982). Regardless of the original function or anatomical

715   connectivity of the linked neuron, the corticospinal interface enabled the linked neuron

716   to innervate the spinal circuits as an artificial corticospinal neuron. Thus, the monkeys

717   were able to modulate stimulation of the preserved spinal cord and wrist torque of the

718   paralyzed hand by modulating the firing rate of the artificial corticospinal neuron. This

719   result suggests the corticospinal interface replaced the function of the corticospinal tract

720   after SCI. However, the innate corticospinal tract and corticospinal interface do not

721   perform exactly the same function, i.e., the innate corticospinal tract does not activate

722   afferent fibers, while the corticospinal interface does. Conversely, the activation of

723   afferent fibers has a strong impact on the spinal circuits, which in turn generate a

724   powerful motor output, thereby boosting the weakened motor output after SCI. Another

725   difference is the delay of muscle activation. The latency of muscle activation from

726   spikes of the linked neurons via the corticospinal interface (ave. $\pm$ s.d.: 53.0 $\pm$ 16.6 ms,

727   range: 9-119 ms) was longer than that of innate corticospinal neurons innervating the

728   forearm muscles of monkeys (3–18 ms) (Fetz and Cheney, 1980). The reason for the

729   longer delay via the corticospinal interface might be because a 50-ms time window was

730   used to average the firing rates of the linked neurons to achieve smoother changes in the

731   stimulus parameters. Such a long latency may be solvable by improving the

732   computational performance of the interface.

733 In our study, task performance in conjunction with the corticospinal interface was
734 similarly achieved irrespective of the original firing patterns of the linked neurons
735 before the corticospinal interface trials (Fig. 4B). This indicates that the modulation of
736 linked neurons is flexible and might be to some degree independent of their original
737 firing patterns, which is consistent with previous studies demonstrating flexibility in
738 controlling the firing rates of M1 cells (Fetz, 1969; Moritz et al., 2008). Thus, the
739 corticospinal interface enabled the direct control of residual spinal circuits connected to
740 the linked neurons and triggered the modulation of their firing pattern to regain
741 impaired motor function after SCI.

742 Brain-controlled functional electrical stimulation of muscles can be used to control the
743 magnitude of the stimulus-induced forces in a paralyzed upper limb (Moritz et al., 2008;
744 Pohlmeyer et al., 2009; Kato et al., 2019). However, muscle stimulation activates the
745 motor end plates or muscle fibers directly. Hence, muscular contraction is accomplished
746 with an inverted recruitment order in which large diameter muscle fibers are activated
747 preferentially, which is the opposite order from the physiological condition, thereby
748 preventing smooth force control (McNeal and Reswick, 1976). In contrast, spinal
749 stimulation recruits motoneurons trans-synaptically via afferent fibers (Mushahwar and
750 Horch, 2000; Aoyagi et al., 2004; Bamford et al., 2005; Gaunt et al., 2006; Kato et al.,
751 2019; Greiner et al., 2021; Kaneshige et al., 2022), so that motoneurons are activated in
752 the natural order (Henneman, 1957; Henneman et al., 1965), which, in turn, may
753 produce graded muscle contractions. Furthermore, spinal stimulation simultaneously
754 activates excitatory and inhibitory interneurons to motoneurons (Nishimura et al., 2013;
755 Guiho et al., 2021; Kaneshige et al., 2022) in the flexor and extensor muscles (Moritz et
756 al., 2007; Nishimura et al., 2013; Greiner et al., 2021; Kaneshige et al., 2022),
757 suggesting brain-controlled spinal stimulation via the corticospinal interface modulates
758 force output by a similar mechanism that is closer to the physiological condition than
759 via muscle stimulation.

760

761 **4.3 Unlinked neurons**

762 We previously demonstrated that closed-loop muscle stimulation using cortical
763 oscillations induces targeted spatial changes in cortical activity in extensive areas. The
764 strongest modulation of high-gamma activity became localized around an arbitrarily-

765 selected cortical site that controls stimulation (Kato et al., 2019). Although cortical
766 oscillations, such as high-gamma activity, are thought to reflect the activity of neural
767 assemblies in regions neighboring the recording site, it remains unclear how the
768 neuronal activity of individual neurons is changed to incorporate the neural interface.
769 Since we used a multi-electrode array, which allowed us to record assemblies of M1
770 neurons, we investigated how the unlinked neurons, which were not connected to the
771 interface, modulated their activity in response to the corticospinal interface.

772 We found three types of unlinked neurons: "task-unrelated," "increased," and
773 "decreased." The firing rates of the "increased" and "decreased" unlinked neurons were
774 modulated similarly to the linked neurons according to the required magnitude of wrist
775 torque (Fig. 7A). Since the activity of the "increased" unlinked neurons was associated
776 with the activity of the linked neurons, they might have similar functions, e.g., they
777 have similar preferred directions and/or receive a common upstream input. The activity
778 of the "decreased" unlinked neurons showed the opposite activity pattern to the linked
779 and "increased" unlinked neurons, which may indicate that there is reciprocal
780 innervation between "decreased" unlinked neurons and a subgroup of linked neurons
781 and "increased" unlinked neurons. Some "task-unrelated" unlinked neurons changed
782 their firing characteristics to those of "task-related" neurons and became either
783 "increased" or "decreased" neurons according to the demands of the task, i.e., weak or
784 strong torque (Figs. 7F, 8B, 8H). These subpopulations have presumably higher
785 thresholds and receive common inputs with subpopulations that already exhibit either
786 "increasing" or "decreasing" activity when weak torque is required.

787 The modulation of the unlinked neurons during the catch trials tended to be smaller than
788 during the corticospinal interface trials (Catch in Figs. 5A, 6B, 6H). This result suggests
789 that many "task-related" neurons were affected by spinal cord stimulation via
790 projections from the preserved ascending pathway, leading to the increased modulation
791 of their activity during the corticospinal interface trials.

792

4.4 Clinical perspective and prospect

794 Of those people who survive a stroke, only 40–70% regain upper limb dexterity
795 (Houwink et al., 2013). The major challenge in the field of neuroprosthetics is to restore

27

796   dexterous finger movements and functionally coordinated multi-joint movements. The

797   use of brain-controlled functional electrical stimulation of muscles should be effective

798   in such cases, and previous studies have shown the restoration of a series of functional

799   goal-directed limb movements (Ethier et al., 2012; Bouton et al., 2016). However, to

800   induce functional movement of multiple joints, many electrodes must be implanted into

801   many muscles. In contrast, spinal stimulation with a single electrode on the cervical

802   cord evokes facilitative or suppressive responses in multiple muscles, including those

803   located on proximal and distal joints, and activates synergistic muscle groups. For

804   example, stimulation strongly facilitates finger flexor muscles, while it suppresses the

805   antagonist muscles, which leads to coordinated movements similar to natural voluntary

806   movements (Nishimura et al., 2013; Kato et al., 2019). Spinal stimulation may be a

807   suitable target for restoring natural limb movements such as dexterous finger control

808   and coordinated multi-joint movements of the hand-arm-shoulder. Since we used a

809   single signal derived from the M1 to control stimulation of a spinal site, the degree of

810   movement control demonstrated here remains limited (Figs. 1, 3). Extending our

811   paradigm to the control of more natural and complex movements would require

812   additional input signals from unlinked neurons including increased, decreased, and

813   unrelated types, and output to multiple spinal sites on rostral-caudal placements as well

814   as ventral-dorsal placements of the spinal cord.

815   Since a substantial portion of the dorsal column sending somatosensory information

816   upstream was lesioned in our SCI model (Fig. 1C), the somatosensory function of the

817   limb on the lesioned side seemed to be impaired (see 3.1 in the Results) and the

818   monkeys might not have used somatosensory information for torque control. In the

819   present study, the monkeys obtained visual feedback about the produced torque,

820   suggesting that visual feedback might have compensated for the lost proprioceptive

821   feedback. Actually, the monkeys were over-trained to perform the same task before SCI,

822   and showed better task performance than with the corticospinal interface after SCI (see

823   3.3 in the Results), indicating that the associations between residual functions such as

824   the level of effort required to exert torque and visual feedback of the exerted torque had

825   already been well-established and might have been maintained even after SCI.

826   Somatosensory feedback is essential for the efficient and accurate control of force

827   output and object manipulation. SCI and stroke commonly cause somatosensory

828   dysfunction in addition to motor dysfunction. However, no therapeutic treatment for

829   somatosensory dysfunction exists. Prior work has shown that direct cortical stimulation

830   of the primary somatosensory cortex induces an artificial somatosensory perception

831   according to somatotopy. Furthermore, there is a linear relationship between current

832   intensity and the perceived intensity of the evoked sensation (Johnson et al., 2013;

833   Hiremath et al., 2017; Lee et al., 2018; Kirin et al., 2019). These results suggest that the

834   modulation of stimulation parameters such as current intensity and frequency to the

835   primary somatosensory cortex can provide somatosensory feedback for tactile

836   information and contact force in real time. The possibility of closing the loop for a

837   bidirectional sensory-motor neuroprosthesis by coupling stimulation-evoked

838   somatosensory feedback with real-time brain control of a paralyzed hand should be

839   investigated in a future study.

840

841 **Conflict of Interest**

842 The authors declare that the research was conducted in the absence of any commercial
843 or financial relationships that could be construed as a potential conflict of interest.

844

845 **Author contributions**

846 K.O. and Y.N. conceived and designed the experiment. K.O., M.K., M.S., and Y.N.
847 performed the surgeries. K.O. conducted the experiments. K.O., O.Y., and M.K.
848 analyzed the results. K.O., M.K., T.T., and Y.N. wrote the manuscript. All authors have
849 read and approved the final version of the manuscript and agree to be accountable for all
850 aspects of the work in ensuring that questions related to the accuracy or integrity of any
851 part of the work are appropriately investigated and resolved. All persons designated as
852 authors qualify for authorship, and all those who qualify for authorship are listed.

853

862

863 **References**

864 Adrian, E.D., Bronk, D.W., 1929. The discharge of impulses in motor nerve fibres. J.
865 Physiol. 67, i3-151.

866 Ajiboye, A.B., Willett, F.R., Young, D.R., Memberg, W.D., Murphy, B.A., Miller, J.P.,
867 Walter, B.L., Sweet, J.A., Hoyen, H.A., Keith, M.W., Peckham, P.H., Simeral, J.D.,
868 Donoghue, J.P., Hochberg, L.R., Kirsch, R.F., 2017. Restoration of reaching and
869 grasping movements through brain-controlled muscle stimulation in a person with
870 tetraplegia: a proof-of-concept demonstration. The Lancet 389, 1821–1830. doi:
871 /10.1016/S0140-6736(17)30601-3

872 Alam, M., Garcia-Alias, G., Shah, P.K., Gerasimenko, Y., Zhong, H., Roy, R.R.,
873 Edgerton, V.R., 2015. Evaluation of optimal electrode configurations for epidural spinal
874 cord stimulation in cervical spinal cord injured rats. J. Neurosci. Methods 247, 50–57.
875 doi: 10.1016/j.jneumeth.2015.03.012

876 Angeli, C.A., Edgerton, V.R., Gerasimenko, Y.P., Harkema, S.J., 2014. Altering spinal
877 cord excitability enables voluntary movements after chronic complete paralysis in
878 humans. Brain 137, 1394–1409. doi: 10.1093/brain/awu038

879 Aoyagi, Y., Mushahwar, V.K., Stein, R.B., Prochazka, A., 2004. Movements elicited by
880 electrical stimulation of muscles, nerves, intermediate spinal cord, and spinal roots in
881 anesthetized and decerebrate cats. IEEE Trans. Neural Syst. Rehabil. Eng. 12, 1–11. doi:
882 10.1109/TNSRE.2003.823268

883 Bamford, J.A., Putman, C.T., Mushahwar, V.K., 2005. Intraspinal microstimulation
884 preferentially recruits fatigue-resistant muscle fibres and generates gradual force in rat.
885 J. Physiol. 569, 873–884. doi: 10.1113/jphysiol.2005.094516

886 Barra, B., Conti, S., Perich, M.G., Zhuang, K., Schiavone, G., Fallegger, F., Galan, K.,
887 James, N.D., Barraud, Q., Delacombaz, M., Kaeser, M., Rouiller, E.M., Milekovic, T.,
888 Lacour, S., Bloch, J., Courtine, G., Capogrosso, M., 2022. Epidural electrical
889 stimulation of the cervical dorsal roots restores voluntary upper limb control in
890 paralyzed monkeys. Nat. Neurosci. 25, 924–934. doi: 10.1038/s41593-022-01106-5

891 Bouton, C.E., Shaikhouni, A., Annetta, N.V., Bockbrader, M.A., Friedenberg, D.A.,
892 Nielson, D.M., Sharma, G., Sederberg, P.B., Glenn, B.C., Mysiw, W.J., Morgan, A.G.,
893 Deogaonkar, M., Rezai, A.R., 2016. Restoring cortical control of functional movement
894 in a human with quadriplegia. Nature 533, 247–250. doi: 10.1038/nature17435

895 Buys, E.J., Lemon, R.N., Mantel, G.W., Muir, R.B., 1986. Selective facilitation of
896 different hand muscles by single corticospinal neurones in the conscious monkey. J.
897 Physiol. 381, 529–549. doi: 10.1113/jphysiol.1986.sp016342

898   Cheney, P.D., Fetz, E.E., 1980. Functional classes of primate corticomotoneuronal cells
899   and their relation to active force. J. Neurophysiol. 44, 773–791. doi:
900   10.1152/jn.1980.44.4.773

901   Cheney, P.D., Fetz, E.E., Palmer, S.S., 1985. Patterns of facilitation and suppression of
902   antagonist forelimb muscles from motor cortex sites in the awake monkey. J.
903   Neurophysiol. 53, 805–820. doi: 10.1152/jn.1985.53.3.805

904   Cheney, P.D., Kasser, R., Holsapple, J., 1982. Reciprocal effect of single
905   corticomotoneuronal cells on wrist extensor and flexor muscle activity in the primate.
906   Brain Res. 247, 164–168. doi: 10.1016/0006-8993(82)91043-5

907   Ethier, C., Oby, E.R., Bauman, M.J., Miller, L.E., 2012. Restoration of grasp following
908   paralysis through brain-controlled stimulation of muscles. Nature 485, 368–371. doi:
909   10.1038/nature10987

910   Evarts, E.V., 1968. Relation of pyramidal tract activity to force exerted during voluntary
911   movement. J. Neurophysiol. 31, 14–27. doi: 10.1152/jn.1968.31.1.14

912   Fetz, E.E., 1969. Operant conditioning of cortical unit activity. Science 163, 955–958.
913   doi: 10.1126/science.163.3870.955

914   Fetz, E.E., Cheney, P.D., 1979. Muscle fields and response properties of primate
915   corticomotoneuronal cells. Progress in Brain Research, Reflex Control of Posture And
916   Movement. Elsevier, 50, 137-146. doi: 10.1016/S0079-6123(08)60814-6

917   Fetz, E.E., Cheney, P.D., 1980. Postspike facilitation of forelimb muscle activity by
918   primate corticomotoneuronal cells. J. Neurophysiol. 44, 751–772. doi:
919   10.1152/jn.1980.44.4.751

920   Gad, P., Gerasimenko, Y., Zdunowski, S., Turner, A., Sayenko, D., Lu, D.C., Edgerton,
921   V.R., 2017. Weight bearing over-ground stepping in an exoskeleton with non-invasive
922   spinal cord neuromodulation after motor complete paraplegia. Front. Neurosci. 11, 333.
923   doi: 10.3389/fnins.2017.00333

924   Gaunt, R.A., Prochazka, A., Mushahwar, V.K., Guevremont, L., Ellaway, P.H., 2006.
925   Intraspinal microstimulation excites multisegmental sensory afferents at lower stimulus
926   levels than local α-motoneuron responses. J. Neurophysiol. 96, 2995–3005. doi:
927   10.1152/jn.00061.2006

928   Greiner, N., Barra, B., Schiavone, G., Lorach, H., James, N., Conti, S., Kaeser, M.,
929   Fallegger, F., Borgognon, S., Lacour, S., Bloch, J., Courtine, G., Capogrosso, M., 2021.
930   Recruitment of upper-limb motoneurons with epidural electrical stimulation of the
931   cervical spinal cord. Nat. Commun. 12, 435. doi: 10.1038/s41467-020-20703-1

932   Guiho, T., Baker, S.N., Jackson, A., 2021. Epidural and transcutaneous spinal cord
933   stimulation facilitates descending inputs to upper-limb motoneurons in monkeys. J.
934   Neural Eng. 18, 046011. doi: 10.1088/1741-2552/abe358

935   Harkema, S., Gerasimenko, Y., Hodes, J., Burdick, J., Angeli, C., Chen, Y., Ferreira, C.,
936   Willhite, A., Rejc, E., Grossman, R.G., Edgerton, V.R., 2011. Effect of epidural
937   stimulation of the lumbosacral spinal cord on voluntary movement, standing, and
938   assisted stepping after motor complete paraplegia: a case study. The Lancet 377, 1938–
939   1947. doi: 10.1016/S0140-6736(11)60547-3

940   He, S.Q., Dum, R.P., Strick, P.L., 1993. Topographic organization of corticospinal
941   projections from the frontal lobe: motor areas on the lateral surface of the hemisphere. J.
942   Neurosci. 13, 952–980. doi: 10.1523/JNEUROSCI.13-03-00952.1993

943   Henneman, E., 1957. Relation between size of neurons and their susceptibility to
944   discharge. Science 126, 1345–1347. doi: 10.1126/science.126.3287.1345

945   Henneman, E., Somjen, G., Carpenter, D.O., 1965. Functional significance of cell size
946   in spinal motoneurons. J. Neurophysiol. 28, 560–580. doi: 10.1152/jn.1965.28.3.560

947   Hiremath, S.V., Tyler-Kabara, E.C., Wheeler, J.J., Moran, D.W., Gaunt, R.A., Collinger,
948   J.L., Foldes, S.T., Weber, D.J., Chen, W., Boninger, M.L., Wang, W., 2017. Human
949   perception of electrical stimulation on the surface of somatosensory cortex. PLOS ONE
950   12, e0176020. doi: 10.1371/journal.pone.0176020

951   Houwink, A., Nijland, R.H., Geurts, A.C., Kwakkel, G., 2013. Functional recovery of
952   the paretic upper limb after stroke: Who regains hand capacity? Arch. Phys. Med.
953   Rehabil. 94, 839–844. doi: 10.1016/j.apmr.2012.11.031

954   Inanici, F., Samejima, S., Gad, P., Edgerton, V.R., Hofstetter, C.P., Moritz, C.T., 2018.
955   Transcutaneous electrical spinal stimulation promotes long-term recovery of upper
956   extremity function in chronic tetraplegia. IEEE Trans. Neural Syst. Rehabil. Eng. 26,
957   1272–1278. doi: 10.1109/TNSRE.2018.2834339

958   Johnson, L.A., Wander, J.D., Sarma, D., Su, D.K., Fetz, E.E., Ojemann, J.G., 2013.
959   Direct electrical stimulation of somatosensory cortex in humans using
960   electrocorticography electrodes: a qualitative and quantitative report. J. Neural Eng. 10,
961   036021. doi: 10.1088/1741-2560/10/3/036021

962   Kakei, S., Hoffman, D.S., Strick, P.L., 1999. Muscle and movement representations in
963   the primary motor cortex. Science 285, 2136–2139. doi: 10.1126/science.285.5436.2136

964   Kaneshige, M., Obara, K., Suzuki, M., Tazoe, T., Nishimura, Y., 2022. Tuning of motor
965   outputs produced by spinal stimulation during voluntary control of torque directions in
966   monkeys. eLife 11, e78346. doi: 10.7554/eLife.78346

967   Kasten, M.R., Sunshine, M.D., Secrist, E.S., Horner, P.J., Moritz, C.T., 2013.
968   Therapeutic intraspinal microstimulation improves forelimb function after cervical
969   contusion injury. J. Neural Eng. 10, 044001. doi: 10.1088/1741-2560/10/4/044001

970   Kato, K., Nishihara, Y., Nishimura, Y., 2020. Stimulus outputs induced by subdural
971   electrodes on the cervical spinal cord in monkeys. J. Neural Eng. 17, 016044. doi:
972   10.1088/1741-2552/ab63a3

973   Kato, K., Sawada, M., Nishimura, Y., 2019. Bypassing stroke-damaged neural pathways
974   via a neural interface induces targeted cortical adaptation. Nat. Commun. 10, 4699. doi:
975   10.1038/s41467-019-12647-y

976   Kirin, St.C., Yanagisawa, T., Oshino, S., Edakawa, K., Tanaka, M., Kishima, H.,
977   Nishimura, Y., 2019. Somatosensation evoked by cortical surface stimulation of the
978   human primary somatosensory cortex. Front. Neurosci. 13:1019. doi:
979   10.3389/fnins.2019.01019.

980   Lee, B., Kramer, D., Armenta Salas, M., Kellis, S., Brown, D., Dobreva, T., Klaes, C.,
981   Heck, C., Liu, C., Andersen, R.A., 2018. Engineering artificial somatosensation through
982   cortical stimulation in humans. Front. Syst. Neurosci. 12, 24. doi:
983   10.3389/fnsys.2018.00024

984   Lemon, R.N., Mantel, G.W., Muir, R.B., 1986. Corticospinal facilitation of hand
985   muscles during voluntary movement in the conscious monkey. J. Physiol. 381, 497–527.
986   doi: 10.1113/jphysiol.1986.sp016341

987   Lu, D.C., Edgerton, V.R., Modaber, M., AuYong, N., Morikawa, E., Zdunowski, S.,
988   Sarino, M.E., Sarrafzadeh, M., Nuwer, M.R., Roy, R.R., Gerasimenko, Y., 2016.
989   Engaging cervical spinal cord networks to reenable volitional control of hand function
990   in tetraplegic patients. Neurorehabil. Neural Repair 30, 951–962. doi:
991   10.1177/1545968316644344

992   Mcneal, D.R., Reswick, J.B., 1976. Control of skeletal muscle by electrical stimulation,
993   in: Brown, J.H.U., Dickson, J.F. (Eds.), Advances in Biomedical Engineering. Academic
994   Press, 6, 209–256. doi: 10.1016/B978-0-12-004906-6.50010-5

995   Minassian, K., Jilge, B., Rattay, F., Pinter, M.M., Binder, H., Gerstenbrand, F.,
996   Dimitrijevic, M.R., 2004. Stepping-like movements in humans with complete spinal
997   cord injury induced by epidural stimulation of the lumbar cord: electromyographic
998   study of compound muscle action potentials. Spinal Cord 42, 401–416. doi:
999   10.1038/sj.sc.3101615

1000   Mondello, S.E., Kasten, M.R., Horner, P.J., Moritz, C.T., 2014. Therapeutic intraspinal
1001   stimulation to generate activity and promote long-term recovery. Front. Neurosci. 8. doi:
1002   10.3389/fnins.2014.00021

1003   Moritz, C.T., Lucas, T.H., Perlmutter, S.I., Fetz, E.E., 2007. Forelimb movements and
1004   muscle responses evoked by microstimulation of cervical spinal cord in sedated
1005   monkeys. J. Neurophysiol. 97, 110–120. doi: 10.1152/jn.00414.2006

1006   Moritz, C.T., Perlmutter, S.I., Fetz, E.E., 2008. Direct control of paralysed muscles by
1007   cortical neurons. Nature 456, 639–642. doi: 10.1038/nature07418

1008   Mushahwar, V.K., Horch, K.W., 2000. Muscle recruitment through electrical stimulation
1009   of the lumbo-sacral spinal cord. IEEE Trans. Rehabil. Eng. 8, 22–29. doi:
1010   10.1109/86.830945

1011   Musienko, P.E., Pavlova, N.V., Selionov, V.A., Gerasimenko, I., 2009. Locomotion
1012   induced by epidural stimulation in decerebrate cat after spinal cord injury. Biofizika 54,
1013   293–300.

1014   Nishimura, Y., Perlmutter, S.I., Fetz, E.E., 2013. Restoration of upper limb movement
1015   via artificial corticospinal and musculospinal connections in a monkey with spinal cord
1016   injury. Front. Neural Circuits 7. doi: 10.3389/fncir.2013.00057

1017   Perlmutter, S.I., Maier, M.A., Fetz, E.E., 1998. Activity of spinal interneurons and their
1018   effects on forearm muscles during voluntary wrist movements in the monkey. J.
1019   Neurophysiol. 80, 2475–2494. doi: 10.1152/jn.1998.80.5.2475

1020   Pohlmeyer, E.A., Oby, E.R., Perreault, E.J., Solla, S.A., Kilgore, K.L., Kirsch, R.F.,
1021   Miller, L.E., 2009. Toward the restoration of hand use to a paralyzed monkey: Brain-
1022   controlled functional electrical stimulation of forearm muscles. PLoS ONE 4, e5924.
1023   doi: 10.1371/journal.pone.0005924

1024   Razavian, R.S., Dreyfuss, D., Katakura, M., Horwitz, M.D., Kedgley, A.E., 2022. An in
1025   vitro hand simulator for simultaneous control of hand and wrist movements. IEEE
1026   Trans. Biomed. Eng. 69, 975–982. doi: 10.1109/TBME.2021.3110893

1027   Rejc, E., Angeli, C., Harkema, S., 2015. Effects of lumbosacral spinal cord epidural
1028   stimulation for standing after chronic complete paralysis in humans. PLoS ONE 10,
1029   e0133998. doi: 10.1371/journal.pone.0133998

1030   Saigal, R., Renzi, C., Mushahwar, V.K., 2004. Intraspinal microstimulation generates
1031   functional movements after spinal-cord injury. IEEE Trans. Neural Syst. Rehabil. Eng.
1032   12, 430–440. doi: 10.1109/TNSRE.2004.837754

1033   Sergio, L.E., Kalaska, J.F., 2003. Systematic changes in motor cortex cell activity with
1034   arm posture during directional isometric force generation. J. Neurophysiol. 89, 212–
1035   228. doi: 10.1152/jn.00016.2002

1036   Toyoshima, K., Sakai, H., 1982. Exact cortical extent of the origin of the corticospinal
1037   tract (CST) and the quantitative contribution to the CST in different cytoarchitectonic
1038   areas. A study with horseradish peroxidase in the monkey. J. Hirnforsch. 23, 257–269.

1039   Usuda, N., Sugawara, S.K., Fukuyama, H., Nakazawa, K., Amemiya, K., Nishimura, Y.,
1040   2022. Quantitative comparison of corticospinal tracts arising from different cortical
1041   areas in humans. Neurosci. Res. 183, 30–49. doi: 10.1016/j.neures.2022.06.008

1042   Zimmermann, J.B., Jackson, A., 2014. Closed-loop control of spinal cord stimulation to
1043   restore hand function after paralysis. Front. Neurosci. 19. 8–87. doi:
1044   10.3389/fnins.2014.00087

1045   Zimmermann, J.B., Seki, K., Jackson, A., 2011. Reanimating the arm and hand with
1046   intraspinal microstimulation. J. Neural Eng. 8, 054001. doi: 10.1088/1741-
1047   2560/8/5/054001

1048

1049 **Tables**
1050 **Table 1. Summary of the experiments**. Electrode 1 was located on the rostral cervical
1051 cord (C6 rostral), and electrode 6 was located on the caudal cervical cord (T1 rostral). In
1052 the Target column, 2 and 3 indicate a two-graded task and three-graded task, respectively.

Monkey	post-SCI day	Cortical linked neuron	Spinal site (Figure 1D)	Stim. intensity (mA)		Number of targets
				I_0	I_{Max}	
	8	ch26	6	1.50	1.60	2
	9	ch26	6	1.50	1.60	2
	9	ch26	6	1.50	1.60	2
	10	ch26	6	1.30	1.40	2
	11	ch26	6	1.60	1.70	2
	12	ch26	6	1.70	1.80	2
	13	ch26	5	1.70	1.80	2
	14	ch26	5	1.70	1.80	2
	15	ch26	5	1.70	1.80	2
	16	ch26	5	1.70	1.80	3
	17	ch26	5	1.70	1.80	3
	17	ch26	5	1.90	2.00	3
	18	ch26	5	1.70	1.80	3
E	18	ch26	5	1.70	1.80	3
	19	ch26	5	2.10	2.20	3
	20	ch26	5	2.10	2.20	3
	21	ch26	5	1.90	2.00	3
	22	ch26	5	2.30	2.40	3
	23	ch26	5	2.30	2.40	3
	24	ch26	5	2.30	2.40	3
	25	ch26	5	2.30	2.40	3
	26	ch26	5	2.30	2.40	3
	27	ch26	5	2.00	2.10	2
	27	ch26	5	2.30	2.40	2
	28	ch26	5	2.30	2.40	2
	29	ch26	5	2.20	2.30	3
	30	ch26	5	2.20	2.30	3

31	ch26	4	2.90	3.00	3
34	ch26	4	3.10	3.20	2
35	ch26	4	3.10	3.20	2
37	ch26	4	3.10	3.20	2
38	ch26	4	3.10	3.20	2
39	ch96	4	3.10	3.60	2
40	ch78	4	2.50	3.00	2
41	ch78	4	2.30	2.90	2
42	ch78	4	2.30	2.50	2
42	ch78	4	2.50	2.60	2
43	ch78	4	2.50	2.60	2
44	ch78	4	2.50	2.60	2
46	ch78	4	2.50	2.60	2
2	ch42	6	1.40	1.50	2
3	ch42	6	1.40	1.70	2
3	ch38	6	1.40	1.50	2
6	ch14	6	1.10	1.80	2
9	ch72	6	1.50	1.66	2
10	ch72	6	1.80	2.02	2
11	ch72	6	1.42	2.00	2
12	ch72	6	1.36	1.60	2
13	ch72	6	1.44	1.60	2
15	ch72	6	1.60	1.90	2
18	ch72	6	1.50	2.00	2
20	ch62	6	1.50	1.60	2
21	ch62	6	1.50	1.70	2
22	ch62	6	1.46	1.60	2
23	ch62	6	1.50	1.60	2
24	ch62	6	1.44	1.66	2
25	ch62	6	1.60	1.90	2
26	ch62	6	1.70	1.90	2
28	ch62	5	1.48	1.58	3
30	ch62	5	1.10	1.36	3

L

31	ch62	5	1.10	1.38	3
32	ch62	5	1.10	1.26	3
33	ch62	5	1.10	1.30	3
Total	11 pairs			63 sessions	

1053

1054

1055   **Figures**
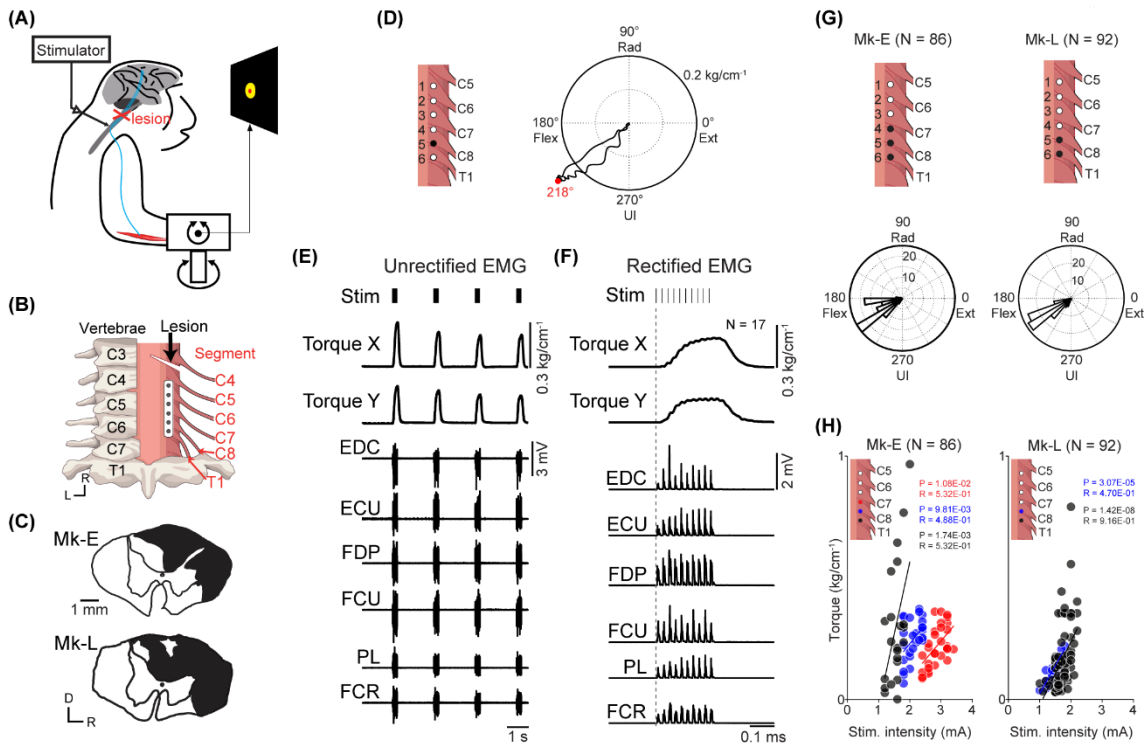
1056

1057   **Figure 1. Motor output evoked by subdural spinal stimulation during rest in awake**
1058   **monkeys with SCI. (A)** A subdural 6-electrode array (platinum) was chronically
1059   implanted over the dorsal-lateral aspect of the cervical spinal cord and placed on the C6–
1060   T1 segments. A slit at the C4/C5 segment indicates the lesion site. **(B)** Lesion extent (black
1061   hatch) at the C4/C5 segment in individual monkeys. **(C)** Subdural spinal stimulation was
1062   applied at rest. **(D)** Typical example of average wrist torque trajectory for tonic spinal
1063   cord stimulation of C8 (black circle, electrode no. 5). Horizontal and vertical components
1064   in this trace correspond to Torque X and Torque Y in Fig. 1F, respectively. Red dot on the
1065   torque trajectory represents the maximum magnitude of the evoked torque. **(E)** Raw traces
1066   of wrist torque and EMG during subdural spinal stimulation of C8. Stimuli consisting of
1067   10 constant-current biphasic square-wave pulses of 40 Hz with a duration of 0.2 ms and
1068   interval of 2 s were delivered through an electrode (Monkey E, post-SCI day 15). **(F)**
1069   Stimulus-triggered averages of wrist torque and rectified EMG. The vertical dashed gray
1070   lines represent the onset of a stimulus train. **(G)** Population data for the directions of the
1071   evoked torque induced by subdural spinal stimulation at rest. Top: black dots on the spinal
1072   cord indicate the stimulation sites. Bottom: histograms indicate the directions of the
1073   evoked wrist torque. **(H)** The relationship between the magnitude of the evoked wrist
1074   torque and stimulus intensity. Colored dots in the figures correspond to spinal stimulus
1075   sites. Significant positive correlations between the magnitude of evoked the torque and
1076   current intensity were found, shown as solid lines (Pearson correlation coefficient; $P <$
1077   0.05).

1078
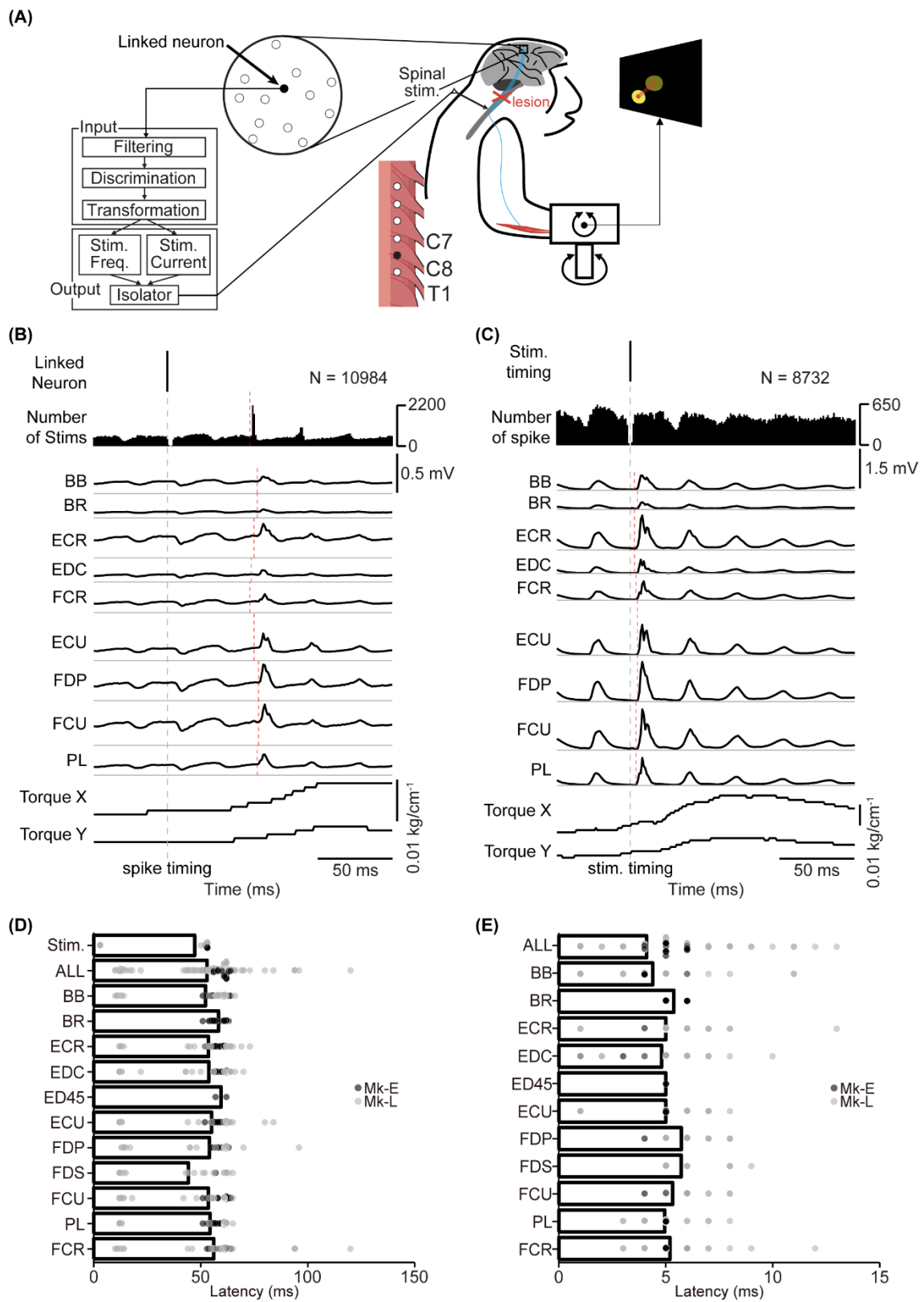
1080 **Figure 2. The corticospinal interface. (A)** Design of the corticospinal interface that
1081 translates the activity of a linked neuron to electrical stimulation of the cervical
1082 enlargement. **(B)** Typical examples of spike-triggered averages (SpTAs) of rectified EMG
1083 traces and torque while a linked neuron was connected to the spinal site via the
1084 corticospinal interface. Red plots indicate the onset latency (vertical red dotted line).
1085 Plots were aligned to the spike timing of a linked neuron (vertical dotted line). From the
1086 1st row: spike of the linked neuron (1st row), spinal stimulation (2nd row), rectified EMG
1087 traces (3rd to 11th rows), and wrist torque (12th and 13th rows). **(C)** Typical examples of
1088 stimulus-triggered averages (StTAs) of rectified EMG traces and torque while a linked
1089 neuron was connected to the spinal site via the corticospinal interface. From the 1st row:
1090 spinal stimulation (1st row), spike of the linked neuron (2nd row), EMG traces (3rd to
1091 11th rows), and wrist torque (12th and 13th rows). Red plots indicate the onset latency
1092 (vertical red dotted line). Plots are aligned to the timing of spinal stimulation (vertical
1093 dotted line). The data were obtained from Monkey E. **(D)** The onset latency of the spinal
1094 stimulation and rectified EMGs from the spike of a linked neuron (ALL: N = 563, PL,
1095 ECU and ECR: N = 62, FDS: N = 24, FDP and EDC: N = 61, ED45: N = 2, BR: N = 40,
1096 others: N = 63 [Monkey E, ALL: N = 360, FDS and ED45: N = 2, FDP and EDC: N =
1097 38, others: N = 40; Monkey L, ALL: N = 203, PL, FDS, ECU and ECR: N = 22, ED45
1098 and BR: N = 0, others: N = 23]). Bars indicate mean values. **(E)** The onset latency of the
1099 rectified EMGs from the spinal stimulation (ALL: N = 567, FDS: N = 25, FDP and EDC:
1100 N = 61, ED45: N = 2, BR: N = 40, others: N = 63 [Monkey E, ALL: N = 360, FDS and
1101 ED45: N = 2, FDP and EDC: N = 38, others: N = 40; Monkey L, ALL: N = 207, ED45
1102 and BR: N = 0, others: N = 23]). Bars indicate mean values.
1103
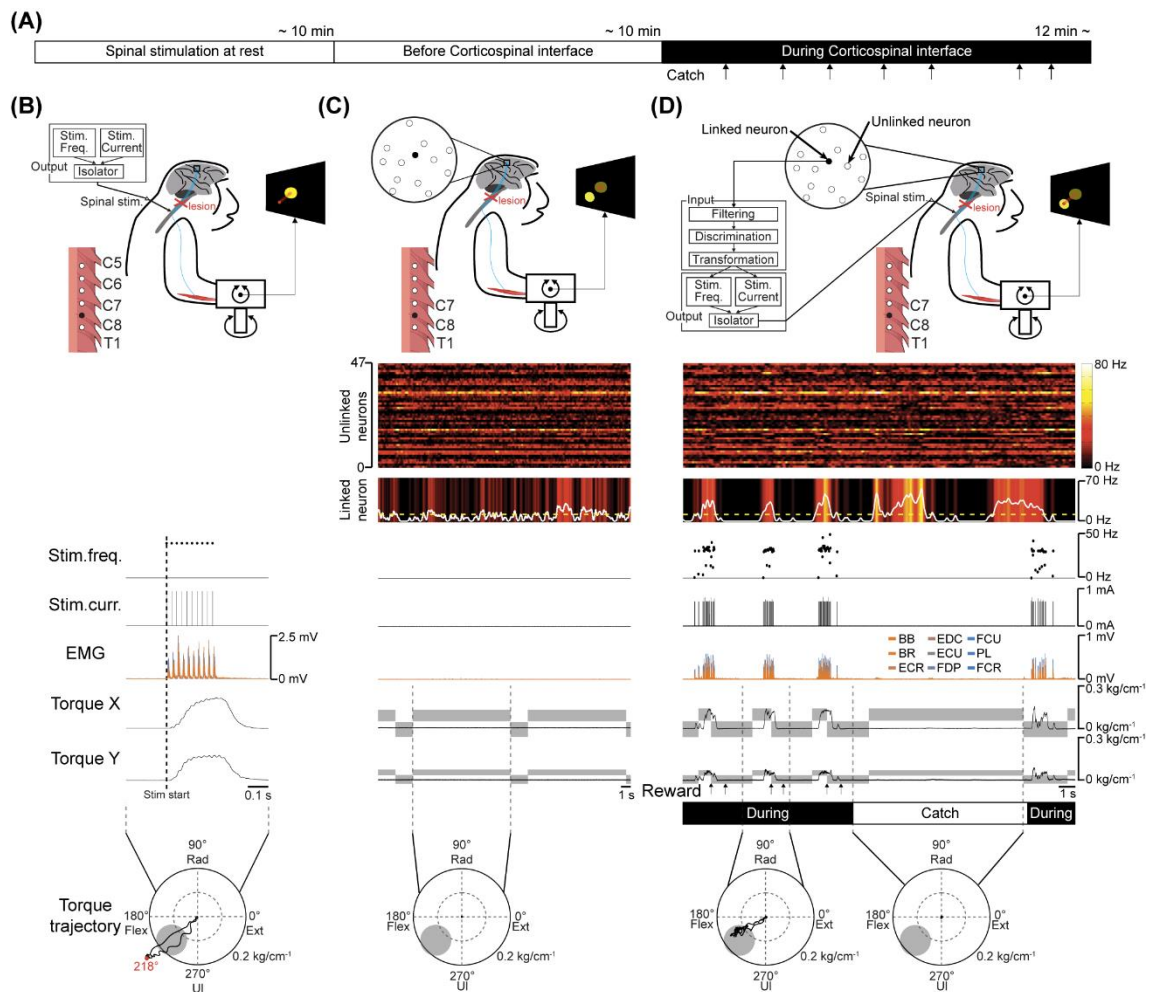
1104
Figure 3. Volitional control of a paralyzed forearm using the corticospinal interface.
(A) Experimental procedure. First, an experiment of "Spinal stimulation at rest" was
conducted to confirm the direction and magnitude of the evoked wrist torque induced by
tonic spinal stimulation at rest. Next, the monkeys performed the torque-tracking task
without the corticospinal interface as an experiment of "Before corticospinal interface".
Subsequently, a linked neuron was connected to the spinal site via the interface, which
was called an experiment of "During corticospinal interface". Catch trials (upward
arrows) were interleaved at random intervals. **(B)** An example of an experiment of "Spinal
stimulation at rest". EMG and wrist torque were produced by stimulation of C8 at 1.8 mA
and 40 Hz. The peripheral target position (gray circle in two-dimensional plot of wrist
torque) was set in the same direction as the evoked torque and at a location at which half
of the maximum magnitude of evoked torque was required. **(C)** An example of an
experiment of "Before corticospinal interface". The monkeys controlled the position of a
cursor (red circle) using wrist torque to acquire targets (yellow circle) displayed on the
screen. The activity of a single neuron (linked neuron, black) in the hand area of M1 was
detected in order to utilize its neuronal activity as an input source for controlling the
stimulation of a single spinal site (black) in the next experiment of "During corticospinal
interface". **(D)** An example of an experiment of "During corticospinal interface",
including three successful trials when the corticospinal interface was on (During, 8th row)
and one catch trial when it was switched off (Catch, 8th row). The modulation of 48

1125   neurons (1st and 2nd rows) was detected through the Utah array in M1 and the activity of
1126   a single neuron (linked neuron, 2nd row) was selected from them as the input signal for
1127   controlling stimulus frequency (3rd row) and intensity (4th row) via the corticospinal
1128   interface. Stimulation frequency and current were determined according to the firing rate
1129   of the linked neuron above a stimulation threshold (yellow dashed line in the 2nd row).
1130   The gray rectangles in the wrist torque traces (6th and 7th rows) represent the peripheral
1131   and center targets. The arrows at the bottom indicate successful trial completion and the
1132   delivery timing of the juice reward (7th row).

1133
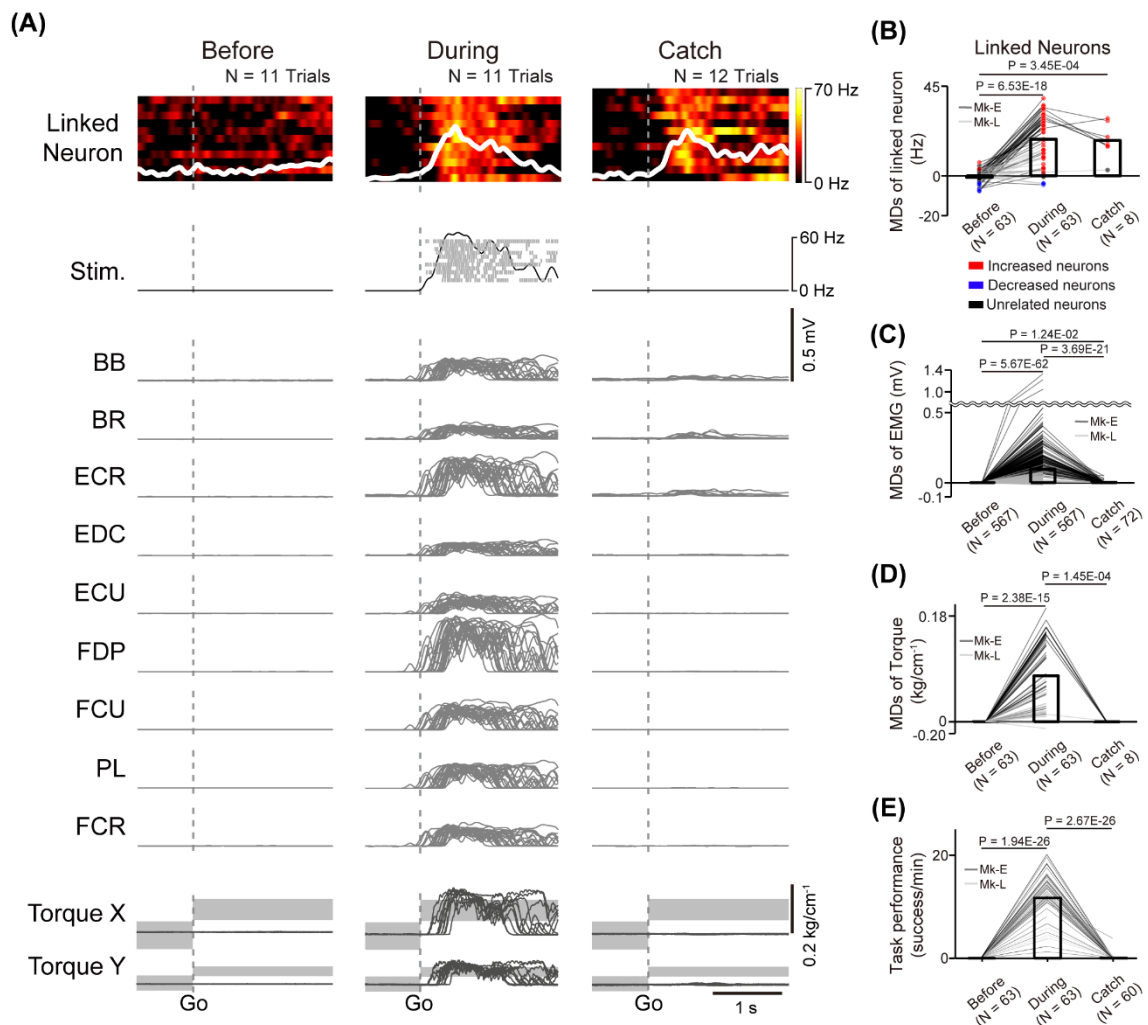
1134

Figure 4. Task-related modulation of linked neurons, EMG, and torque. (A) Examples of the firing rate in individual trials (heatmap) and the average firing rate (white trace) of a linked neuron (1st row), spinal stimulation (2nd row), EMG of the forelimb (3rd to 11th rows), and wrist torque (12th and 13th rows) before (left panel) and during the corticospinal interface (center panel) and catch trials (right panel). Plots are aligned to the timing of target appearance, indicated by the vertical dotted lines. The gray-shaded rectangles in the bottom traces represent the target range of the required torque for a successful trial. **(B–D)** MDs of the firing rates of linked neurons (B), EMG (C), and wrist torque (D) before (left bar) and during the corticospinal interface (center bar) and catch trials (right bar) (N = 63 sessions before and during corticospinal interface, 8 sessions during catch trials [Monkey E, N = 40 sessions before and during corticospinal interface, 7 sessions during catch trials; Monkey L, N = 23 sessions before and during corticospinal interface, 1 session during catch trials]). Bars indicate mean values. Black horizontal lines represent significant differences ($P < 1.67 \times 10^{-2}$ by paired t-test with Bonferroni's correction). Colors of the circles represent the neuron types sorted in each condition (i.e., before and during corticospinal interface and catch trials). Sessions with at least nine trials in each condition were included in the analysis. **(E)** Task performance before and during the corticospinal interface trials and during the

1153 catch trials (N = 63 sessions before and during corticospinal interface, 60 sessions
1154 during catch trials [Monkey E, N = 40 sessions before and during corticospinal
1155 interface, 38 sessions during catch trials; Monkey L, N = 23 sessions before and during
1156 corticospinal interface, 22 sessions during catch trials]). Bars indicate mean values.
1157 Black horizontal lines represent significant differences (P < 1.67×10^{-2} by paired *t*-test
1158 with Bonferroni's correction for *post hoc* multiple comparisons). Sessions with at least
1159 one trial in each condition were included in the analysis.

1160
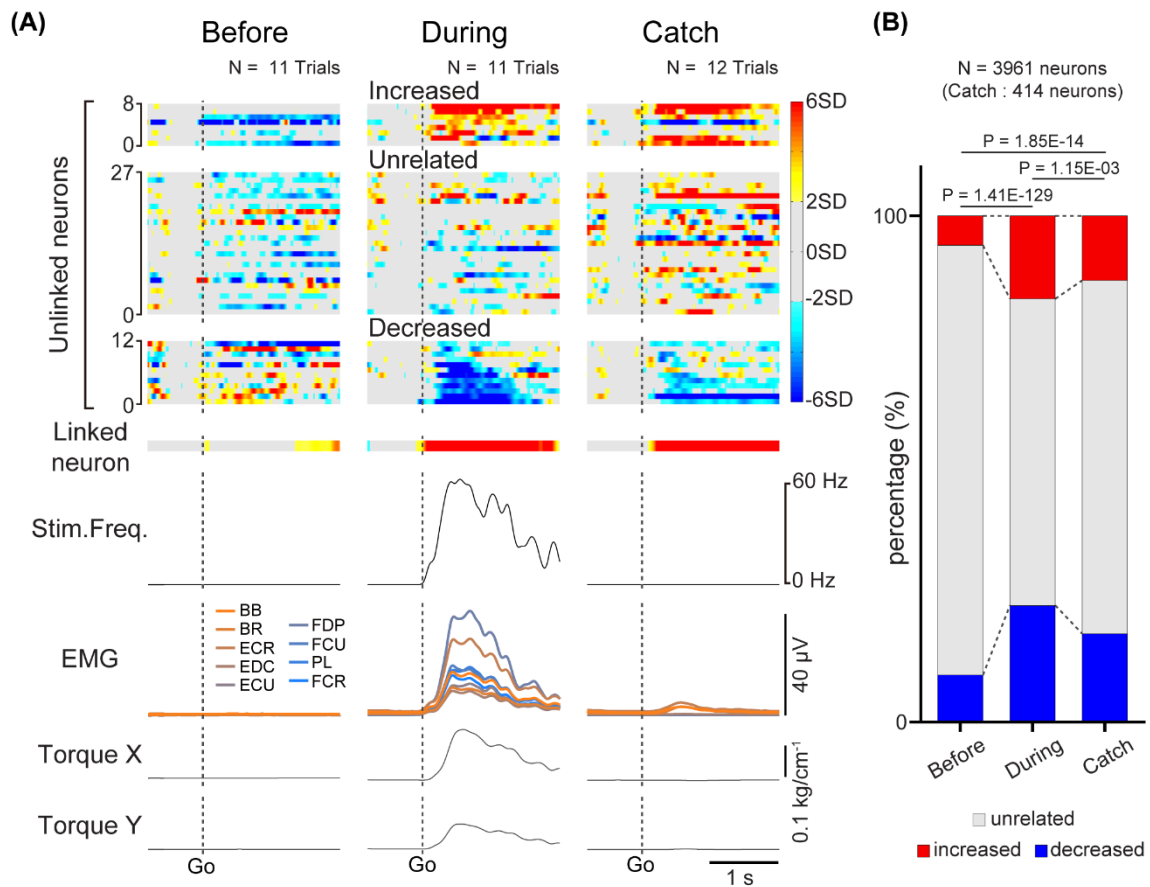
Figure 5. Task-related modulation of unlinked neurons. (A) Examples of average firing rate of M1 cells (1st and 2nd rows), stimulus frequency (3rd row), EMG of the forelimb (4th row), and wrist torque (5th and 6th rows) before (left panel) and during the corticospinal interface trials (center panel) and during the catch trials (right panel). Z-scored firing rates of unlinked (1st row) neurons and linked (2nd row) neurons are shown. Unlinked neurons are sorted into "increased," "decreased," and "unrelated" neurons according to activity during the corticospinal interface sessions. Plots are aligned to the timing of target appearance ("Go"), indicated by the vertical dotted lines. **(B)** The percentage of the types of unlinked neurons (red: "increased" neuron, black: "unrelated" neuron, blue: "decreased" neuron) before and during the corticospinal interface and catch trials. Black horizontal lines represent significant differences ($P < 1.67 \times 10^{-2}$ by chi-squared test with Bonferroni's correction for *post hoc* multiple comparisons).

47
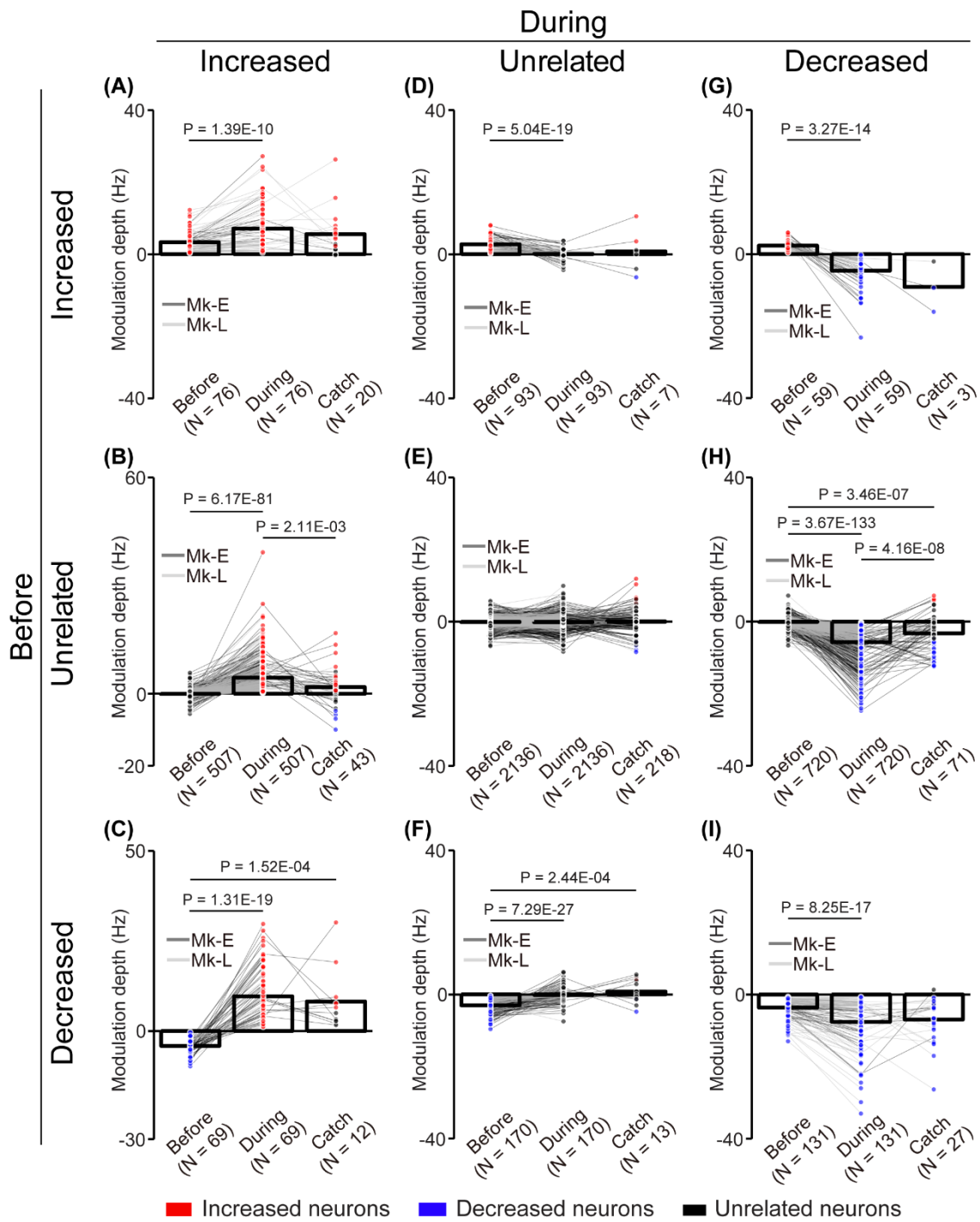
Figure 6. Change of the MDs of unlinked neurons with the corticospinal interface.
(A) Neurons maintained their properties as "increased" type before and during the
corticospinal interface trials. **(B)** Neurons changed their properties from "unrelated" to
"increased" type. **(C)** Neurons changed their properties from "decreased" to "increased"
type. **(D)** Neurons changed their properties from "increased" to "unrelated" type. **(E)**
Neurons maintained their properties as "unrelated" type. **(F)** Neurons changed their

48

1182   properties from "decreased" to "unrelated" type. **(G)** Neurons changed their properties
1183   from "increased" to "decreased" type. **(H)** Neurons changed their properties from
1184   "unrelated" to "decreased" type. **(I)** Neurons maintained their properties as "decreased"
1185   type. Bars and circles indicate the MDs of mean values and individual neurons,
1186   respectively. Colors (red: increased neuron, black: unrelated neuron, blue: decreased
1187   neuron) of the circles represent the neuron type sorted in each condition (i.e.,
1188   experiments of before and during the corticospinal interface and catch trials). Black
1189   horizontal lines represent significant differences ($P < 1.67 \times 10^{-2}$ by paired *t*-test with
1190   Bonferroni's correction for *post hoc* multiple comparisons). Experiments with at least
1191   nine trials were included in each condition.

1192
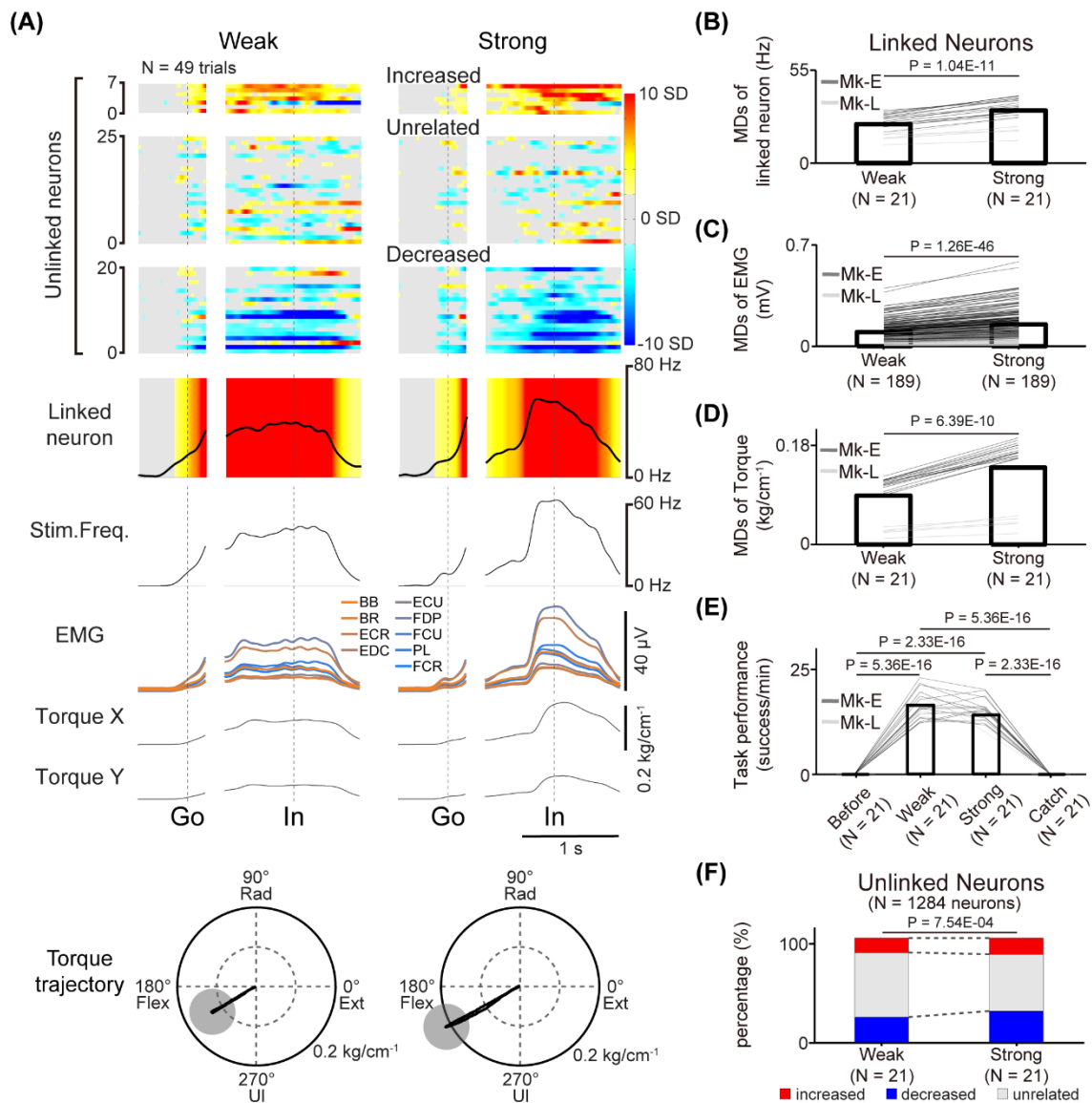
Figure 7. Volitional control of a paralyzed forearm during a three-graded torque-tracking task with the corticospinal interface. (A) Examples of the average M1 firing rate (1st and 2nd rows), stimulus frequency (3rd row), EMG of the forelimb (4th row), and wrist torque (5th and 6th rows) in the weak torque trials (left panel) or strong torque trials (right panel) for a representative session. Heatmap indicates Z-scored firing rates of unlinked and linked neurons. Plots are aligned when the peripheral target appeared ("Go") or when the cursor entered the peripheral target ("In"), indicated by the vertical dotted lines. Torque trajectories are two-dimensional plots of the average wrist torque in the weak torque trials (left) and strong torque trials (right). The gray circles represent the targets of peripheral wrist torque. **(B–F)** Change of M1 neurons, EMG, wrist torque, and task performance during the three-graded torque-tracking task (N = 21 sessions in the weak and strong torque trials [Monkey E, N = 16 sessions; Monkey L, N = 5 sessions]). Black horizontal lines represent significant differences. Bars in (B–F) indicate mean values. **(B)** According to the increase of the required torque, the MDs of the linked

1208   neurons increased (P < 0.05 by paired *t*-test). **(C and D)** Statistical analysis: P < 0.05 by
1209   paired *t*-test. **(E)** Task performance during the corticospinal interface trials was
1210   significantly higher than before the corticospinal interface trials and during the catch trials
1211   (P < 8.33 × 10^{-3} by paired *t*-test with Bonferroni's correction for *post hoc* multiple
1212   comparisons). **(F)** The percentage of increased and decreased neurons was increased in
1213   the strong torque trials (P < 0.05 by chi-squared test).

1214
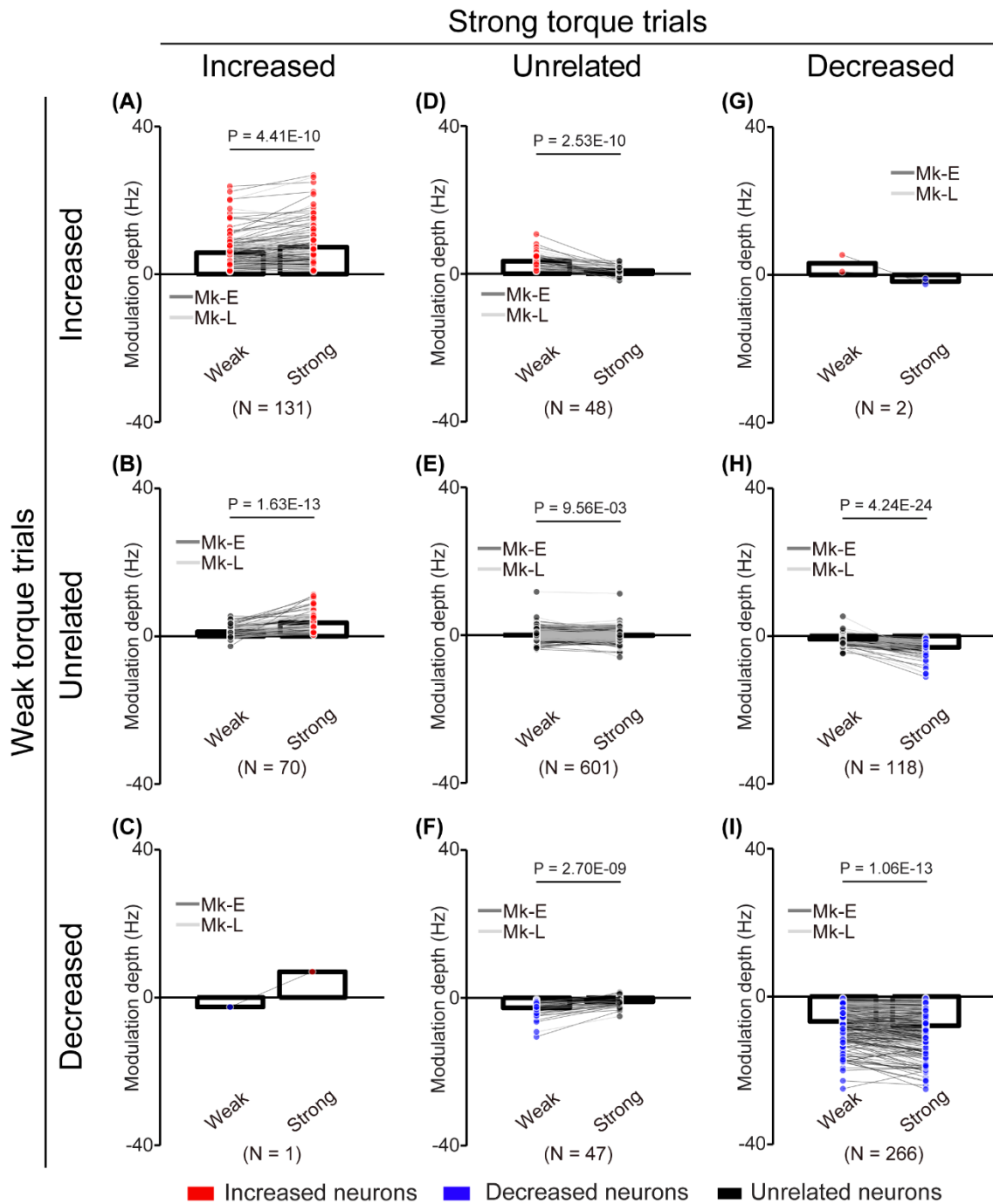
1215

Figure 8. Change of the MDs of unlinked neurons at different torque requirements.
(A) Neurons maintained their properties as "increased" type throughout the experiments.
(B) Neurons changed their properties from "unrelated" to "increased" type. **(C)** Neurons
changed their properties from "decreased" to "increased" type. **(D)** Neurons changed their
properties from "increased" to "unrelated" type. **(E)** Neurons maintained their properties
as "unrelated" type. **(F)** Neurons changed their properties from "decreased" to "unrelated"
type. **(G)** Neurons changed their properties from "increased" to "decreased" type. **(H)**
Neurons changed their properties from "unrelated" to "decreased" type. **(I)** Neurons

1224   maintained their properties as "decreased" type. Bars and circles indicate the MDs of
1225   mean values and individual neurons, respectively. Colors (red: increased neuron, black:
1226   unrelated neuron, blue: decreased neuron) of the circles represent the neuron types sorted
1227   in each condition (i.e., before and during the corticospinal interface and catch trials).
1228   Black horizontal lines represent significant differences ($P < 0.05$ by paired t-test with
1229   Bonferroni's correction). Experiments with at least nine trials were included in each
1230   condition.

1231
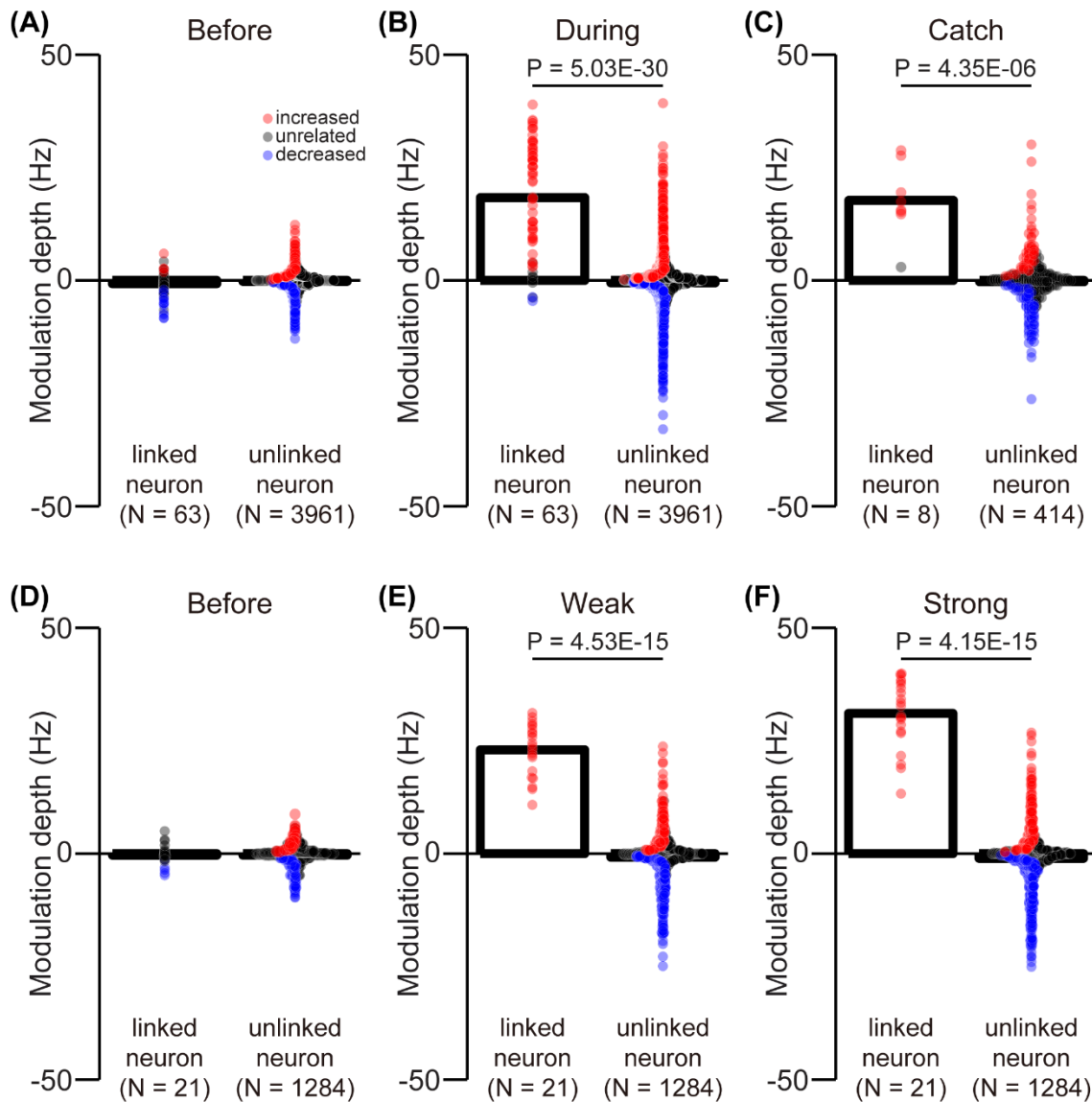
Figure 9. Difference between the MDs of linked and unlinked neurons. The MDs of linked and unlinked neurons before **(A)** and during the corticospinal interface trials **(B)** and during catch trials **(C)**. The MDs of linked and unlinked neurons before the corticospinal interface trials **(D)** and during weak **(E)** and strong trials **(F).** Bars and circles indicate the MDs of mean values and individual neurons, respectively. Colors (red: increased neuron, black: unrelated neuron, blue: decreased neuron) of the circles represent the neuron types sorted in each condition (i.e., before and during the corticospinal interface and catch trials). Black horizontal lines represent significant differences (P < 0.05 by Wilcoxon rank-sum test). Experiments with at least nine trials were included in each condition.